Mineralogical and Hydrogeochemical Characterization of Legacy Mine Wastes near Cobalt, ON

By

Cole Fischer (M.Sc. Candidate)

Supervisors: Dr. Tom Al, Dr. Danielle Fortin

Department of Earth and Environmental Sciences, Advanced Research Complex

University of Ottawa, Ottawa, Ontario

Submitted in conformity with the requirements for the degree of Master of Sciences (Chemical and Environmental Toxicology)

November 2022

Abstract

Cart Lake, located 1.6 km south of the town of Cobalt, ON, contains elevated concentrations of As (0.95 to 18.05 mg/L As_t) resulting from uncontained mine tailings deposited during a silver mining boom from 1910 to 1983. Aqueous geochemical and investigations indicate tailings are sulfate-affected but subject to extensive carbonate buffering, with pH ranging from 6.7 to 8.6, Eh ranging from 46 to 210 mV, and alkalinity ranging from 32 to 201 mg/L HCO_3^-. The dominant cation species are Ca (4.9 to 192.0 mg/L), K (1.1 to 13.5 mg/L), Mg (1.2 to 8.7 mg/L), and Na (2.1 to 16.9 mg/L) and the dominant anionic species are alkalinity, As (0.003 to 18.1 mg/L), Cl^- (0.3 to 16.8 mg/L), PO_4 (0.04. to 9.6 mg/L), and SO_4^{2-} (6.8 to 456.1 mg/L). Concentrations of minor and trace cations such as Fe, Co, and Ni are present at the μg/L scale. Mineralogical investigations suggest As is mobilized from primary reactive sulfide and arsenide minerals such as arsenopyrite, skutterudite, and safflorite/löllingite/ rammelsbergite solid solutions. Primary mineral alteration products including Ca-Fe arsenates and erythrite are found in these tailings, resulting from direct alteration from primary minerals and precipitation from solution respectively. Secondary Ca-Fe arsenates and Co-Arsenates attenuate As, Co, and Fe by absorption and coprecipitation throughout the tailings profile, influenced by the presence of alteration rims around reactive mineral grains in the vadose zone. Field analysis of cation speciation and geochemical modelling of elemental equilibrium concentrations with weathering primary mineral surfaces would further inform conclusions regarding the relative contributions of each mineral to total As attenuation.

Le lac Cart , situé à 1,6 km au sud de la ville de Cobalt en Ontario contient des concentrations élevées d'arsenic (As) (0,95 à 18,05 mg/L) résultant de la déposition de résidus miniers non confinés pendant une période d'extraction d'argent entre 1910 et 1983. Les analyses de géochimie aqueuse indiquent que les niveaux de sulfate présents dans les résidus ont été atténués par la présence de minéraux carbonatés. Les eaux souterraines ont un pH entre 6.7 et 8.6, un potentiel redox (Eh) entre 46 et 210 mV et une alcalinité entre 32 et 201 mg/L HCO3-. Les espèces cationiques dominantes sont Ca (4.9 à 192.0 mg/L), K (1.1 à 13.5 mg/L), Mg (1.2 à 8.7 mg/L) et Na (2.1 à 16.9 mg/L) et les espèces anioniques dominantes sont l'alcalinité, As (0.003 à 18.1 mg/L), Cl- (0.3 à 16.8 mg/L), PO4 (0.04 à 9.6 mg/L) et SO42- (6.8 à 456.1 mg/L). Les concentrations de cations mineurs et traces (tels que Fe, Co et Ni) sont présentes à l'échelle du □g/L. Les analyses minéralogiques suggèrent que As provient des minéraux primaires riches en S et des minéraux contenant de l'arsenic comme l'arsénopyrite, la skutterudite et les solutions solides de safflorite/löllingite/rammelsbergite. Les produits d'altération des minéraux primaires y compris les arséniates de Ca-Fe et l'érythrite se trouvent dans ces résidus résultant respectivement de l'altération directe des minéraux primaires et de la précipitation en solution. Les arséniates Ca-Fe secondaires et les Co-arsénates atténuent As, Co et Fe par absorption et coprécipitation dans tout le profil des résidus. L'analyse sur le terrain de la spéciation des cations et la modélisation géochimique des concentrations en équilibre avec l'altération des surfaces minérales primaires éclaireraient les conclusions concernant les contributions relatives de chaque minéral relative à l'atténuation totale de l'arsenic.

Acknowledgements

This endeavor would not have been possible without the expertise of Dr. Tom Al and Dr. Danielle Fortin, and the support of the Department of Earth & Environmental Sciences at the University of Ottawa. I am also thankful to Jean Percival and Alexandre Desbarats of NRCAN, Story Environmental, and Agnico Eagle for their support during the planning phases of this project. Lastly, a huge thank you to my amazing brothers, sisters-in-law, parents, and girlfriend for keeping me fed and motivated throughout the course of this project.

Table of Contents

List of Figures

List of Tables

1 Introduction

Improperly stored and treated mine wastes pose a threat to human health around the world. Mine wastes are managed federally and provincially/territorially in Canada, with the Canadian Council of Ministers for the Environment (CCME) providing a universal standard. Many provinces and territories develop and enforce their own mine waste management standards, which are applied additionally to the federal standards. To date, no international body regulates these wastes, resulting in a disparity in treatment effectiveness and compliance from country to country.

Canadian regulations regarding mine wastes have changed dramatically over the last century as the chemical processes that determine the toxicity of these wastes have become better understood. Due to Canada's long and varied history in natural resource extraction, federal and provincial/territorial governments allocate significant budgetary resources to cleaning up sites left in their respective responsibilities. Currently, the federal government assumes responsibility for almost all legacy mine waste sites decommissioned before regulations necessitated cleanup by the mine operators themselves.

Cobalt, located in the mid-latitudes of Ontario, is an example of a legacy mining camp for which the federal government has assumed the bulk of the responsibility for monitoring and remediation. Discovery of vein mineralization hosting silver (Ag) and cobalt (Co) in the Cobalt Mining Camp (CMC) (comprising modern Cobalt, New Liskeard, and Haileybury) led to Cobalt's rapid development into the (briefly) largest producer of silver in the world, with peak production exceeding 31.5 million oz. in 1911 (Petruk et al., 1971). As surficial and shallow underground deposits were exhausted, mining activity gradually wound down and eventually ceased completely with the exception of the occasional hobbyist enterprise. With the increasing popularity of electric cars, the Co frequently found in the vein mineralizations gains greater economic importance setting the stage for another economic boom.

The residues from the early period of mining activity are widespread and continue to cause problems to the modern CMC municipalities. Tailings from mill sites in the area

were deposited uncontained into local surface water systems, a practice which led to widespread environmental impacts that have been under study since contamination levels were established (Dumaresq 2005; Kelly, Champagne, and Michel 2007; Kwong et al. 2007; Percival et al. 2007; Sprague and Vermaire 2018; Sprague, Michel, and Vermaire 2016). The primary contaminants of concern associated with these wastes are mercury (Hg), cyanide (CN^-), and arsenic (As), of which As is the primary subject of discussion in the present study due to the lack of Hg and CN^- in the Cart Lake tailings resulting from flotation separation milling practices. Arsenic is a well-known toxic element and carcinogen sourcing from ore minerals, mobilized by milling and oxidation during post-depositional weathering processes (Dumaresq 2005; Kelly, Champagne, and Michel 2007; Kwong et al. 2007; Percival et al. 2007; Sprague and Vermaire 2018; Sprague, Michel, and Vermaire 2016).

Extensive work has been carried out in the CMC regarding the mobilization and distribution of toxic elements and the harmful potential of other mine residues (Clarke 2017; Kelly, Champagne, and Michel 2007; Kwong et al. 2007; Percival et al. 2007; Sprague and Vermaire 2018; Sprague, Michel, and Vermaire 2016). These studies span a range of locations and scopes of research, but all agree that residual mine wastes pose a potential threat to human health and local environmental integrity. To date, none of these studies have investigated the interactions of aqueous ion speciation, primary reactive mineral alteration, and secondary mineral development in the vadose and saturated zones of the Cart Lake tailings deposit in the CMC. The interactions of secondary mineralizations and tailings pore water likely exert an effect on the fate of As in the system.

This study was carried out with the assistance and funding of NRCAN/RNCAN, specifically Alex Desbarats and Jeanne Percival, both employees of NRCAN with experience in the Cobalt area. Field work for this study was conducted in the fall of 2019, with one visit in September and one in October. An additional field visit was planned for the fall season of 2020, but due to travel restrictions regarding COVID-19 this trip was cancelled.

1.1 Arsenic in Mine Wastes

Arsenic is a common constituent of the hydrothermal-origin ore veins found in the CMC. Due to its low market value at the time of tailings deposition, As was rarely recovered and was usually disposed of as a waste product. Modern regulations necessitate the proper storage of As-containing wastes in impermeable storage facilities but during the peak of mining activity in the CMC these regulations did not exist.

In 1998, the World Health Organization (WHO) reduced the acceptable concentration of As in drinking water from 50 µg/L to 10 µg/L, based on newly emerged studies on its carcinogenicity and genotoxicity (World Health Organization 2011).

The mobility and toxicity of As is affected by its oxidation state, a factor influenced by pH, redox potential, solution composition, temperature, and microbial activity (Clarke 2017; Craw and Bowell 2014; Bowell, Morley, and Din 1994;). Arsenic is released through the alteration and dissolution of minerals such as arsenopyrite, skutterudite, and scorodite which readily release As into solution via oxidative weathering where geochemical conditions allow (Bowell et al. 2014). Arsenic concentrations may be attenuated by adsorption, co-precipitation, or interactions with organic matter as water flows through a sediment profile (Bowell et al. 2014).

The speciation of As at 25ºC and 1 bar, with a total As concentration of 10^{-6} M, is presented in Figure 1. (Lu and Zhu 2011).

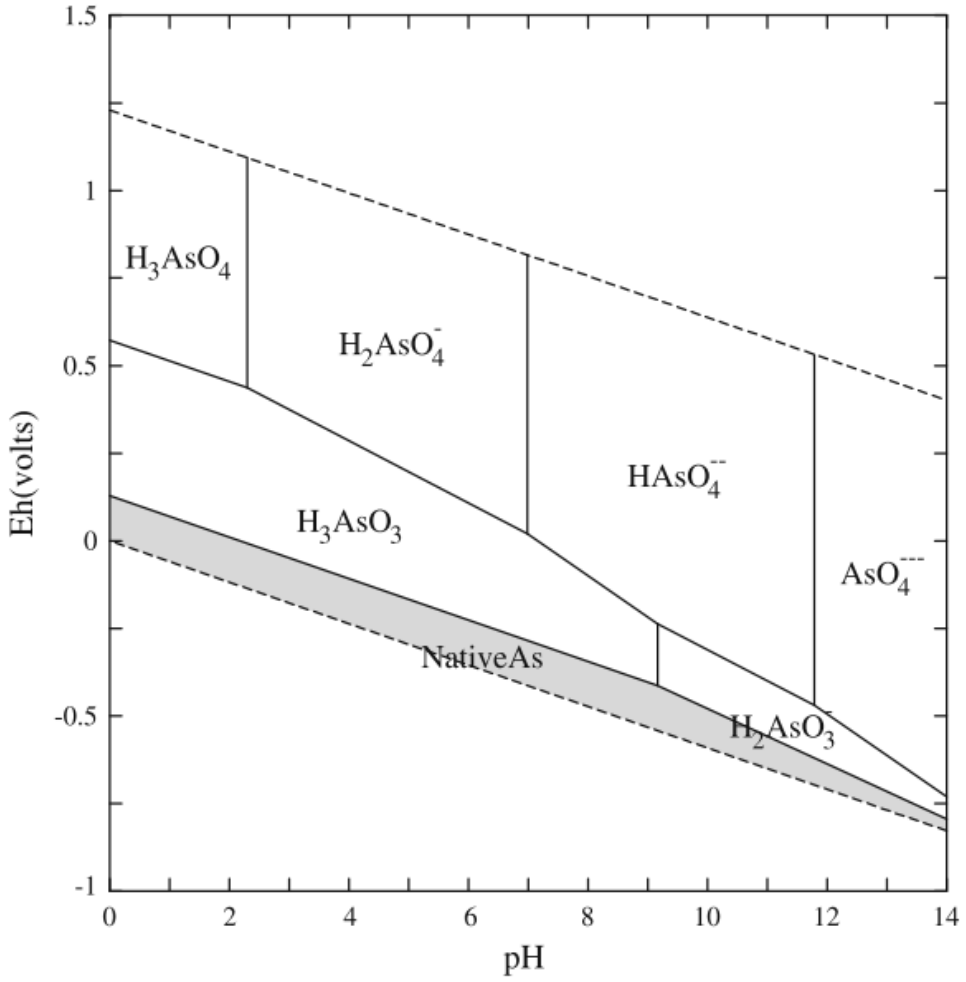

*Figure 1 - Eh-pH diagram for the system As-O-H, 25*C, 1 bar (Lu and Zhu, 2011)*

Across these species, As exists as As^{3+} (Arsenite (H_3AsO_3, $H_2AsO_3^-$)) and As^{5+} (Arsenate (H_3AsO_4, $H_2AsO_4^-$, $HAsO_4^{-2}$, AsO_4^{-3}) which occur as a function of pH and Eh. Organic forms of As, of which the most common is the methylated form, are found as products of detoxification by biological processes. Arsenic with an oxidation state of 0 has never been observed in a stable form (Campbell and Nordstrom 2014).

Trivalent and pentavalent As behave in geochemically similar manners to aqueous phosphate and boron respectively (Campbell and Nordstrom 2014). Arsenic oxyanions form complexes with many common major and trace elements found in mine tailings

environments, such as Ca, Na, K, Mg, Al, Co, Fe, Mn, Ni, and others (Campbell and Nordstrom 2014). Based on the fact that As^{5+} has a stronger positive charge, it forms aqueous ion complexes with metals more readily than the lesser charged As^{3+} (Campbell and Nordstrom 2014).

The presence and relative abundancies of Fe(II) and Fe(III) also influence the speciation and associated toxicity of As. Ferric iron oxidizes As, reducing to Fe^{2+} and is regenerated through biological processes (Nordstrom 2003). Oxidized As binds readily to reaction sites on surfaces in contact with the solution leading to the precipitation of a characteristic set of secondary mineral precipitates. These reactions can be mediated, and sometimes dominated, by microorganisms as discussed in section 1.3.

1.1.1 Controls on Arsenic Mobilization

Redox potential, pH, Fe/Al-hydroxide content, microbiological communities, and major cation/anions concentrations influence mobility, transportation, and attenuation of As in natural and contaminated areas, factors (Campbell and Nordstrom 2014; Lu and Zhu 2011; Bowell et al. 2014; Masscheleyn, et. al. 1991; Nordstrom et al. 2014). Under reducing conditions (Eh<0 mV), most As is generally found in As^{3+} form, whereas in more oxidizing conditions (Eh>0 mV), higher proportions of As will be found as As^{5+} (Marin et al. 1993). This represents a simplification of the complex geochemical environments found in most mine-waste-related settings, where weathering and elevated concentrations of other reactive elements can influence concentration and speciation.

The majority of As released to groundwater occurs as a result of weathering of primary As-containing minerals such as skutterudite ($CoAs_3$), safflorite/löllingite/rammelsbergite $(Co,Fe,Ni)As_2$ solid solution series, arsenopyrite (FeAsS), langisite (CoAs), orpiment (As_2S_3), realgar (AsS), and others (Clarke 2017). Oxidation reactions involving these types of minerals proceed in the presence of dissolved oxygen (DO) and elevated Fe concentrations commonly found in shallow regions of the water column (Moses et al. 1987). Arsenic released via these reactions is subject to transport in aqueous solution and attenuation (Lengke et al., 2009).

Solution and mineral composition determine whether oxidative dissolution of As-bearing minerals occurs congruently or incongruently. Arsenopyrite has been shown to dissolve congruently in laboratory settings, releasing As^{3+} and As^{5+} in approximately 1:1 molar ratios at circumneutral pH (Walker et al., 2006). Precipitation reactions commonly occur where dissolution is incongruent, involving secondary minerals such as jarosite ($KFe_3(SO_4)_2(OH)_6$ or ferric arsenates (Al et al., 2000; Lengke et al., 2009). In contrast to other As minerals, fluctuations in pH have not been observed to greatly influence rates of arsenopyrite oxidation, although DO and concentrations of dissolved Fe exert a significant effect (Lengke et al. 2009). Oxidation reactions involving other As-bearing minerals such as arsenic trisulfide, realgar, and orpiment are more highly dependent on pH (Lengke et. al., 2009).

Oxidation rates generally increase with temperature for As-bearing sulfide minerals, with some exceptions (Lengke et. al., 2009, Rimstidt et. al., 1993).

Surface Complexation and Sorption

One of the primary pathways for attenuation of As in waters is through surface complexation and sorption. The rates at which these processes occur is dominated by the point of zero net charge (PZNC) for the minerals at the solid-liquid interface, as well as the degree of hydrolysis of those minerals (Campbell and Nordstrom, 2014). Associated solution pH and Eh also influence these reactions. At higher pH levels, As does not sorb as easily to the reactive surface of Fe oxhydroxides, as in higher pH conditions As is mostly found as less positively charged species and is less attracted to negative mineral surface charges.

In environments with high sulfur concentrations, thioarsensenic species become more common. Replacement of O ions by S in As compounds exerts strong control over As speciation (Campbell and Nordstrom 2014).

1.2 Weathering of Primary Minerals and Secondary Mineral Formation

Interactions between tailings minerals and aqueous solutes in groundwater influence the mobility, transport, and fate of weathering products in mine tailings deposits.

As groundwater flows through a porous media, secondary minerals form over time. The types of secondary minerals are dependent on the composition of the groundwater and the nature of reactions with primary minerals, and their importance in understanding impacts to the surrounding environment from tailings weathering is well understood. Petrunic et. al. (2005, 2006), Nordstrom et. al. (2014), Markl et. al. (2014) and Hiller et. al. (2013), among others, have identified the importance of secondary mineralization to the geochemistry of mine wastes and the associated potential for contamination and toxicity. The precipitation and dissolution of secondary minerals influence the aqueous concentrations of metals and their speciation, a relationship that evolves as conditions change (Petrunic et al., 2006). Several reactions in particular exert stronger control over the transport and mobility of dissolved or precipitated toxic elements, as discussed below.

1.2.1 Acid generation and pH Buffering by Mineral Dissolution

One of the most studied and environmentally harmful effects of improperly stored mine wastes is the generation of acidic waters. These acidic waters affect surface and groundwater quality and can render aquatic environments unsuitable for all but the most extremophilic organisms.

Oxidation and dissolution of solid sulfide phases results in the production of sulfate (SO_4^{2-}), ferrous iron (Fe^{2+}) and H^+, decreasing the pH. This reaction proceeds through several intermediate S species, due to limits on the speed of transfer of electrons (Moses et al. 1987). Reaction 1 shows a generic sulfide mineral (pyrite (FeS_2)) reacting with oxygen and water.

$$(\mathbf{1}) \quad 2FeS_{2(s)} + 7O_{2(g)} + 2H_2O_{(l)} \rightarrow oxidation \rightarrow 2Fe^{2+}_{(aq)} + 4SO^{2-}_{4(aq)} + 4H^{+}_{(aq)}$$

1.2.2 Neutralization by Ferrous Iron Oxidation

Ferrous iron (Fe^{2+}) produced during sulfide oxidation can be oxidized by O and excess H ions to produce ferric iron (Fe^{3+}), resulting in a decrease in H^+ ions and subsequent increase in pH. Reaction 2 shows how this reaction proceeds.

$$(\mathbf{2}) \quad 4Fe^{2+}_{(aq)} + O_{2(g)} + 4H^{+}_{(aq)} \rightarrow oxidation \rightarrow 4Fe^{3+}_{(aq)} + 2H_2O_{(l)}$$

1.2.3 Pyrite Oxidation by Ferric Iron

High concentrations of dissolved Fe^{3+} in solutions exposed to pyrite results in further production of H^+ and Fe^{2+} ions and a subsequent decrease in pH, as shown in reaction 3.

$$(\mathbf{3}) \quad FeS_{2(s)} + 14Fe^{3+}_{(aq)} + 8H_2O_{(l)} \rightarrow oxidation \rightarrow 15Fe^{2+}_{(aq)} + 2SO^{2-}_{4(aq)} + 16H^{+}_{(aq)}$$

This reaction occurs significantly faster than the oxidation of pyrite by atmospheric oxygen. Srsenopyrite, one of the reactive minerals expected to be observed in Cart Lake, would follow a similar reaction process yielding additional As into solution.

1.2.4 Net Acid Production

The net effect of these reactions is the production of H^+ ions and a decrease in solution pH. If biologically moderated, these reactions can proceed to extreme extents, resulting in pH values reaching 0 or even below in the absence of buffering materials.

1.2.5 Buffering and Neutralization by Carbonate Minerals

In environments with abundant carbonate minerals such as calcite, significant percentages of the acid generated through sulfide oxidation can be neutralized or even brought to pH values above 7 as presented in equation 4.

$$(\mathbf{4}) \quad CaCO_3 + H^+ \rightarrow neutralization \rightarrow Ca^{2+} + HCO_3^-$$

Carbonate minerals such as calcite act as pH buffers when exposed to acidic or basic waters. Dissolution of these minerals, encouraged by the presence of dissolved atmospheric CO_2, typically yields an increase in $Ca^{2+}_{(aq)}$ or Mg^{2+}concentrations and an increase in pH through the production of bicarbonate ions. The dissolution of a generic carbonate mineral in the presence of dissolved CO_2 is presented in Equation 5.

$$(\mathbf{5}) \quad CaCO_3 + CO_2 + H_2O \rightarrow Ca^{2+} + 2HCO_3^-$$

1.2.6 Primary Mineral Weathering and Secondary Mineral Formation

Al et. al (2000) studied the interactions of carbonate minerals with pore water in sulfide-rich mine tailings in Timmins, ON. This study used Time of Flight Laser Ionization Mass Spectrometry (TOF-LIMS) and Transmission Electron Microscopy (TEM) to identify

the chemical composition and mineralogy of secondary mineral coatings on primary carbonate grains. It was found that acidity generated via oxidation and weathering of sulfide minerals was reduced as water travelled through the tailings, due to the buffering capacity of calcite grains (Al et al., 2000). Accompanying this buffering process was a corresponding decrease in the dissolved concentrations of metals and SO_4^{2-}, resulting from secondary mineral coating formation (Al et al., 2000). The principle processes involved in the removal of dissolved elements from the pore water were adsorption, surface complexation, and co-precipitation (Al et al., 2000). The formation of coatings reduced the rates of mass transfer between mineral species and the surrounding pore water and affected the dissolution/precipitation balance of the primary and secondary minerals found at the site. As these coatings form around a particle, the distance between primary tailings particle cores and the surrounding solutions increases, resulting in a gradual reduction in reaction rates as the thickness of these coatings increase (Al et al., 2000). This study suggests that incorporating incongruent dissolution into conceptual and numerical models would have yielded more accurate results in this case, and that secondary mineral coatings exert a strong control over aqueous ion concentration in tailings pore waters (Al et al., 2000).

Hiller et. al. (2013) studied tailings from a siderite/barite/mercury mine, products of primary minerals also rich in chalcopyrite, pyrite, and arsenopyrite. These tailings are characterized by near-neutral pore water pH, minor solid-phase sulfide concentrations and high solid-phase carbonate concentrations in eastern Slovakia. (Hiller et al. 2013). Any acid generated as a result of sulfide weathering was quickly neutralized by the high carbonate concentration in the tailings (Hiller et al. 2013). Elevated concentrations of (in decreasing order) Fe, Ba, Mn, Cu, Sb, Hg, and As were observed in the tailings pore water, but the mobility of these elements did not follow the total concentration trend (Hiller et al. 2013). Geochemical modeling showed this to be the result of co-precipitation and adsorption of these ions with Fe-oxyhydroxide secondary minerals (Hiller et al. 2013). The degree of As sorption to these minerals estimated using PHREEQC were found to be highly pH-dependent, due to Fe-oxyhydroxide functional groups at the surfaces of these minerals being highly pH-dependent (Hiller et al. 2013).

Filippi et. al. (2015) studied As mobility and secondary mineralogy in a 250 year old carbonate-poor mine tailings deposit in the Czech republic. These tailings were processed from polymetallic (Ag-Ni-Co-Bi-As) hydrothermal veins, similar in composition to the veins found in the CMC. Arsenopyrite, one of the primary reactive minerals remaining in the tailings, weathered over time resulting in the formation of As-bearing secondary minerals such as ferric arsenate, scorodite, and kaňkite (unique to this location) (Filippi et al. 2015). Under the low pH conditions resulting from sulfide oxidation and lack of buffering minerals (pH ≅ 3.3 in the centre of the tailings deposit), the aqueous concentrations of As, Fe, and SO_4^{2-} ions increased significantly. Pore water elemental concentrations were amenable to the precipitation of ferric oxyhydroxides and jarosite, which were estimated using the aqueous geochemical modelling software PHREEQC to be the dominant minerals exerting control on the migration of As into the surrounding environment (Filippi et al. 2015).

The formation of secondary mineral coatings on primary grains is an important process in the control of the transport of aqueous ions. Arsenopyrite, when exposed to reactive atmospheric gases such as O_2, oxidizes to form coatings of Fe-hydroxides, arsenates, or arsenites (Nesbitt and Muir, 1998). Coatings formed by exposure to gases remain extremely thin but are sufficient to almost completely suppress reaction rates one the coatings reach a thickness of 5 nm at which point the layer become effectively passivating (Nesbitt and Muir, 1998). However, when grains of similar composition are reacted in the presence of aqueous solutions, rates of alteration increase greatly due to the compromising of the oxidized barrier layer by other solution components (principally Fe-related) (Buckley and Walker 1988, Nesbitt and Muir, 1998;).

1.3 Geomicrobial Influences on Aqueous Ion Speciation

1.3.1 Geomicrobial Transformation of As

Over 200 strains of bacteria and archaea have been shown to use As^{3+} and As^{5+} as a source of energy through reduction processes, or have been shown to detoxify As through biological processes such as cytoplasmic reduction and excretion using the ArsB protein (Amend et al. 2014). Until relatively recently, microbial activity was suspected to

be the only pathway of arsenite oxidation in natural systems (Nordstrom 2003). Although this is now known to be incorrect, it still accounts for the majority of oxidation in natural systems (Nordstrom 2003). Organisms that utilize As as a part of normal biological functions can be classed generally into four categories (Amend et al. 2014):

1. Arsenate-reducing prokaryotes (DARPs), which obtain energy through the reduction of $As^{5+,}$
2. Chemoautotrophic arsenite oxidizers (CAOs), which gain energy from the oxidation of As^{3+} to $As^{5+,}$ and are usually found in aerobic environments,
3. Heterotrophic arsenite oxidizers (HAOs), which gain energy from the oxidation of As^{3+} to As^{5+}
4. Arsenate-resistant organisms (ARMs), who detoxify As but do not use it in their energy metabolism.

These classifications are determined by whether the organisms use reductive processes for energy metabolism, or simply detoxify As.

Biological reactions involving the transformation of As vary throughout the water column, and change significantly from the oxic to anoxic zone. A study of the Giant mine tailings in the Northwest Territories (NWT) showed low ratios (<1) of As^{5+}:As^{3+} in the anoxic zones and the inverse in the oxic zones, suggesting geomicrobially mediated reduction of As proceeds at lesser rates in the presence of oxygen (Andrade et al. 2010). These findings were corroborated by analysis of the sediment profile in the summer and winter months, with As^{3+} dominating in the colder months (Andrade et al. 2010). This decrease in the proportion of As^{5+} and near depletion of sulfide in colder months is hypothesized to occur as a result of increased rates of microbial As reduction and seasonal cycling of Fe-sulfides (Andrade et al. 2010).

In anaerobic environments, such as those found in the lower portions of some water columns, the dominant fraction of As-utilizing microorganisms anaerobically respire using organic matter as the initial electron donor and As^{5+} as a terminal electron receptor, reducing it to As(III). These organisms use As as an analogue to O_2 in the cellular energy production process.

1.3.2 Geomicrobial Transformation of Fe and SO_4^{2-}

Arguably the most important microbially mediated reactions in mine tailings involve Fe and SO_4^{2-}cycling. These reactions have been shown to be seasonally dependent, mainly due to fluctuations in oxygen content and temperature as a part of freeze-thaw cycles (Casiot et al. 2003; Praharaj and Fortin 2004). Seasonal cycling of Fe, SO_4^{2-}, and S^{2-} has been studied extensively, and it has been observed that SO_4^{2-}, S^{2-}, and Fe are found in higher concentrations in the summer (Praharaj and Fortin 2008). Reduction rates of Fe^{3+} can be dominated by microorganisms or abiotic mineral interactions, depending on the characteristics of the medium in which the reactions are taking place (Praharaj and Fortin 2008). However, biotic rates of oxidation generally exceed those of abiotic mineral interaction by several orders of magnitude (Nordstrom 2003). Iron and SO_4^{2-} reactions occur at variable rates, and through different pathways, depending on the oxygen content of a system. Iron and SO_4^{2-} can both be oxidized in aerobic environments, and ferric iron reduction and S oxidation are known to occur in anaerobic environments (Baker and Banfield 2003).

The oxidation of pyrite, as discussed in section 1.2, is one of the primary drivers of acid mine drainage. This reaction is also highly influenced by geomicrobial activity and must be accounted for when studying aqueous geochemical processes but is difficult to accurately characterize given the high number of abiotic factors influencing these rates. Generally, two hypotheses exist regarding geomicrobial oxidation of pyrite, direct and indirect contact mechanisms. Direct contact oxidation occurs as a result of cell attachment and enzymatic degradation of mineral surfaces, whereas indirect mechanisms occur as a result of cell attachment increasing ferrous-ferric oxidation rates which encourages mineral dissolution (Nordstrom 2003). Scant evidence exists for the direct contact mechanism, and the majority of the literature supports the indirect contact mechanism (Nordstrom 2003). Both hypotheses propose weathering by way of successive pitting on mineral surfaces (Nordstrom 2003).

Reaction rates are highly dependent on the aeration of the sediment, which is influenced by the penetration depth and biological composition of plant root systems. Other controlling factors include the surface area of reactive minerals, pH, and

temperature (Nordstrom 2003). Rates are generally enhanced in mixed microbial cultures rather than monocultures.

1.4 Study Site: Cart Lake, Cobalt, Ontario, Canada

1.4.1 Cart Lake – Location and History

Located approximately 1.6 km south of the town of Cobalt, Cart Lake (Figure 2) was the deposition site of tailings and mill effluents from 1910 to 1983 (Anderson, 1993, Dumaresq, 2005). Four different mills were constructed and operated near Cart Lake, each mill operating for short time periods (generally one to three years, intermittently). These mills employed a variety of ore refinement methodologies and the tailings were frequently recovered, reworked, and redeposited as the efficiency of silver extraction techniques improved. The progression of milling facilities at Cart Lake provides an interesting case study of a period of innovation in the field of ore refinement. The end result of this processing was the reduction in concentration of several toxic elements such as Hg compared to other tailings deposits in the area (Anderson 1993), and a sufficiently low Ag content rendering the likelihood of reprocessing unlikely. However, this processing also resulted in increased concentration and mobility of As in the tailings material due to greater surface area from smaller particle sizes (Dumaresq, 2005, Kwong et al., 2006, Sprague et. al., 2016)

Today only a small area of open water remains near the northern shore. A small, fenced-in headframe still exists on the southern edge of the tailings. The remains of a dam constructed in approximately 1920 to facilitate access to previously deposited tailings can still be seen on site near the southern edge of the lake.

A small stream flowing northward exists on the western margin of the lake but may be ephemeral. The fine to coarse sand particle size distribution of the tailings results in a high degree of infiltration, and the stream and standing water bodies at the site are indicative of the water table's presence close to or above the surface in some areas of the tailings deposit.

Water level measurements from the piezometers sampled during this project do not provide sufficient information to draw groundwater elevation contours in the tailings, as a formal elevation survey of the tops of the piezometers was not carried out during this study. Groundwater contours were produced by Charles Dumaresq, and, at the time of

that sampling program, water levels ranged from 92.4 m above sea level to 91.4 m above sea level, decreasing towards the exposed water at the northern edge of the tailings (Appendix 1) (Dumaresq 2005).

Story Environmental, a consulting firm operating in the Haileybury area, supplied several drill logs taken from the Cart Lake tailings. These logs indicate a tailings depth of approximately 3.5m-4m at their deepest point, evidenced by the occurrence of lake bottom sediments at depth (Story Environmental 2014).

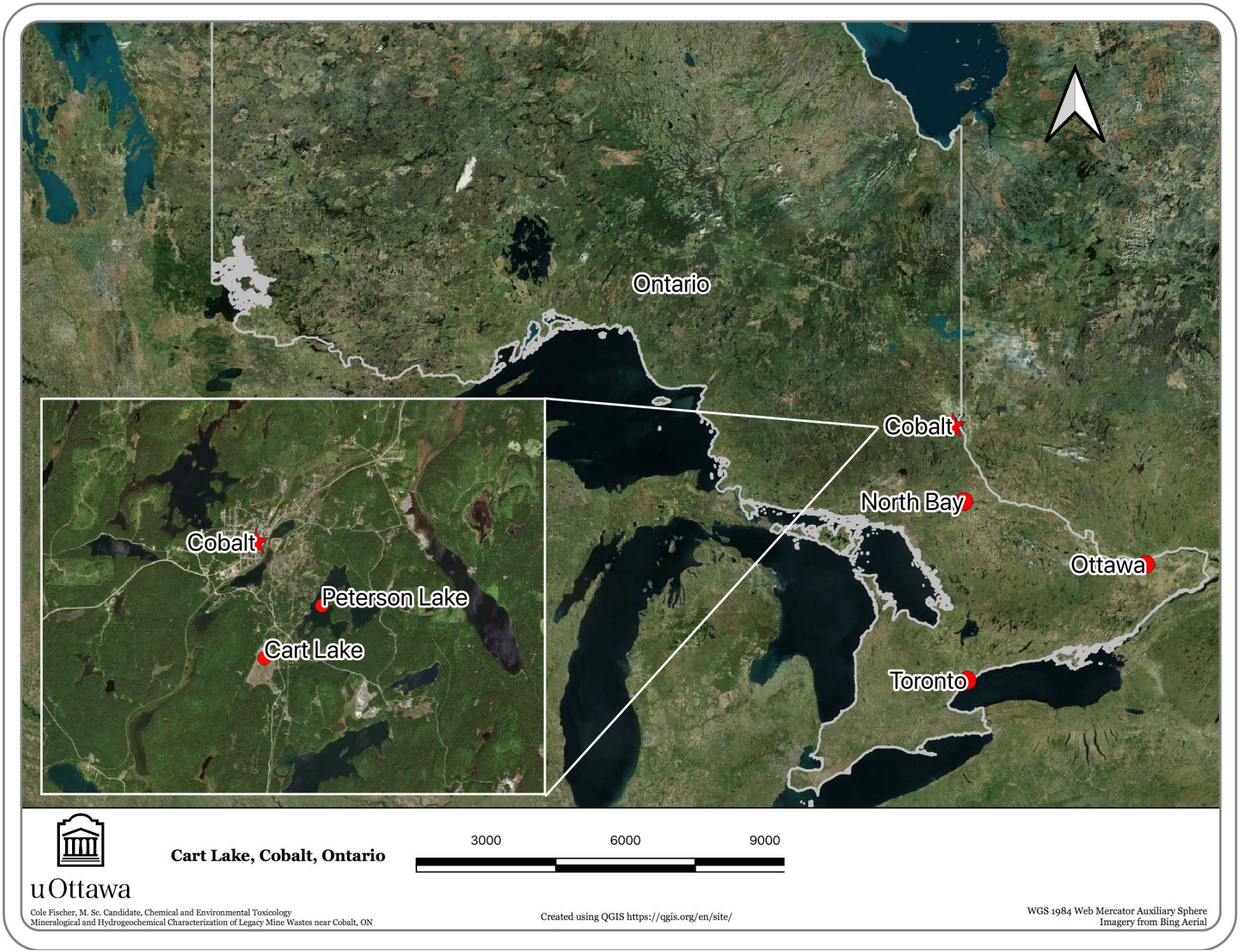

Figure 2 - Map showing Cobalt, ON, and Cart and Peterson Lakes

The tailings themselves are composed principally of coarse to fine sand (60%) and lesser silts and clays (40%) resulting in high infiltration rates and infrequent standing water on the tailings (Anderson, 1985, Sprague and Vermaire 2018; Kramer et al. 1999). Generally, groundwater flow is expected to be to the NNE, down the topographic gradient (Dumaresq, 2005). At the western edge of the tailings, a small stream flows towards the lake at the northern edge of the impoundment.

These tailings have been the site of numerous prior studies characterizing the mineralogical composition (Clarke, 2017; Dumaresq, 2005), tailings groundwater geochemistry (Dumaresq 1993, Percival et. al., 2007, Sprague et. al., 2018), and potential for revegetation (Michel et. al., 2007).

1.4.2 Ore Vein Mineralogy

The fault structures of the CMC exert strong control over the CMC mineralization. The ore-bearing veins in the CMC are polymetallic (Ag-As-Bi-Co-Ni) and are hydrothermal and epigenetic in origin (Kissin 1992; Markl et al., 2016; Scharrer et. al., 2019; Ruzicka and Thorpe, 2015). The polymetallic veins typically originate by infill of dilational spaces caused by fracturing, and rarely, if ever, through alteration of host rocks (Kissin 1992). The ore deposits of the CMC can be divided generally into three categories of mineral assemblages, which are (Petruk 1971b; Ruzicka and Thorpe 2015):

- Base metal-sulfide assemblages, occurring in the Archean basement layers
- Arsenide assemblages, occurring in close proximity to the Nipissing diabase/Huronian sedimentary member contacts and Nipissing diabase/Archean metavolcanic contacts
- Sulfide assemblages in close proximity to fractured arsenide veins

The arsenide assemblages, which contain the highest amounts of Ag, are zoned directionally to the Nipissing diabase sills. Arsenides nearest the sills contain higher concentrations of Ni, with increases in concentration of Co in the intermediate zones and elevated Fe near the sill boundaries (Petruk 1971a). The most common ore-forming minerals are listed in Table 1.

Table 1 - Ore-Forming and Secondary Minerals of the CMC

	Mineral	Formula
Arsenides	Nickeline	NiAs
	Langisite	(Co,Ni)As
	Safflorite	$(Co,Fe,Ni)As_2$
	Loellingite	$FeAs_2$
	Rammelsbergite/ Pararammelsbergite	$NiAs_2$
	Skutterudite	$(Co,Fe,Ni)As_{2-3}$
Sulpharsenides	Cobaltite	(Co,Fe,Ni)AsS
	Gersdorfrite	NiAsS
	Arsenopyrite	FeAsS
	Proustite	Ag_2AsS_3
	Alloclasite	(Fe,Co)AsS
Antimonides	Breithauptite	NiSb
	Ullmannite	NiSbS
	Dyscrasite	Ag_3Sb
	Allargentum	$Ag_{1-X}Sb_X$
Arsenates	Erythrite	$Co_3(AsO_4)_2{\cdot}8H_2O$
	Annabergite	$Ni3(AsO_4)2{\cdot}8H_2O$
	Scorodite	$(Fe,Al)AsO_4{\cdot}2H_2O$
Sulfides	Pyrargyrite	Ag_3SbS_3
	Staphanite	Ag_5SbS_4
	Tetrahedrite	$(Cu,Fe)_{12}Sb_4S_{13}$
	Chalcopyrite	$CuFeS_2$
	Bornite	Cu_5FeS_4
	Galena	PbS
	Marcasite	FeS_2
	Pyrite	FeS_2
	Sphalerite	(Zn,Fe,Mn)S
	Pyrrhotite	$Fe_{1-X}S$
	Acanthite	Ag_2S
	Molybdenite	MoS_2
Oxides	Rutile	TiO_2
	Hematite	Fe_2O_3
	Magnetite	Fe_3O_4
	Anatase	TiO_2
	Ilmenite	$FeTiO_3$
Sulfates	Melanterite	$FeSO_4\ 7H_2O$
	Gypsum	$CaSO_4{\cdot}2H_2O$
Silicates	Quartz	SiO_2
	Chlorite	$(Mg,Fe)_3(SiAl)_4O_{10}(OH)_2(Mg,Fe)_3(OH)_6$
	Albite	$(Na,Ca)(Al,Si)_4O_8$
Carbonates	Calcite	$CaCO_3$
	Dolomite	$CaMg(CO_3)_2$
	Malachite	$Cu_2(CO_3)(OH)_2$
Native Metals	Ag, Au, Bi, As	-

1.4.3 Cart Lake Ore Milling Processes

The four mills constructed on Cart Lake represented a progression in ore refinement technology. The complex nature of the Ag-bearing ores of the CMC provided unique metallurgical challenges, necessitating the incorporation of physical and chemical extraction methods in tandem. The varied milling processes employed at this location impact the current tailings groundwater geochemistry and mineralogy, as well as the mobility and transport of solutes.

Ore Extraction

Access to bedrock was principally achieved through hand digging, and later by high-pressure water scouring, creating an extensive network of trenches across the CMC. With overburden removed, the ground was rapidly but thoroughly inspected for any trace of native silver or indicator minerals such as pink erythrite. Due to the shallow occurrence of many of the veins, deeper mining was not necessary at first. However, as the easily accessible veins were depleted, mine shafts and adits were dug into bedrock, increasing the area's output of valuable metals but leaving behind a labyrinthian network of poorly supported tunnels. This remaining underground network continues to cause problems to the present (Anderson 1993).

Savage Mill (1910-1912)

The Savage Mill, formerly located near the south end of Cart Lake, was the first mill constructed at Cart Lake (Anderson 1993). Incoming ore was hand sorted, with coarser gangue materials discarded, and fine/middling materials crushed and shipped to an off-site concentrator. A tramway was built between this mill and the McKinley-Darragh concentrator, to facilitate the transport of fine and middling tailings (Anderson 1993).

Seneca-Superior Mill (1910-1919, intermittent)

The Seneca-Superior Mill was formerly located on the western edge of Cart Lake, today evidenced only by degraded concrete footings. Incoming ore was hand-sorted, and undersized materials were milled and shipped off-site (Sprague and Vermaire 2018; Anderson 1993). Further concentration capacity was added in 1914 to sort and concentrate Ag from the finely milled products. The mill operated until 1916, closed for a

period of two years, then was reopened and upgraded from 1918-1919 to reprocess tailings previously deposited into the nearby Peterson Lake (Anderson 1993). After processing, the Cart Lake tailings contained approximately 0.3 to 0.5 ounces of Ag per ton of tailings, and approximately 6 ounces of Co per ton of tailings (Anderson, 1993). This mill was abandoned in 1919 (Anderson 1993).

Cobalt Provincial Mill (1911-1938, intermittent)

Constructed in 1911 as a simple hand sorting facility, the Cobalt Provincial mill was upgraded to a gravity concentrator from 1917-1918 (Anderson 1993). Flotation separation capacity was added in 1918, and the milling and flotation facilities were upgraded with more efficient, but similar technologies in 1919 (Anderson 1993). The Cobalt Provincial mill closed in 1920, then was briefly reopened with upgraded facilities in 1938 (Anderson 1993).

Silverfields (Silver Summit) Mill (1963-1983, intermittent)

The Silverfields mill was the last mill to be constructed near Cart Lake, employing gravity and flotation separation methods (Anderson 1993). The mill was closed in 1964, then reopened in 1965 to process surplus ore from the Alexandria property located 1.2 km from the mill site (Anderson 1993). The flotation agents used by this mill extracted the majority of the As contained in the ore minerals concurrently with the Ag, reducing the concentration of As in the deposited tailings relative to other mills operating during this time as the As/Ag-rich concentrates were exported off-site (Anderson 1993). Due to the increased efficiency of the technology, it is estimated that the tailings remaining in Cart Lake contain less than one oz. of silver per ton of material, making their eventual reprocessing unlikely (Anderson 1993).

Cart Lake Milling Processes – Gravity Concentration and Flotation Separation

Every mill associated with the Cart Lake tailings made use of hand sorting, gravity concentration, or flotation separation methods. Hand sorting involved the separation of crushed ore based on visual inspection, whereas gravity sorting leveraged the relatively high density of ore minerals to separate out profitable ore fractions. Flotation separation employed a mixture of emulsifiers such as pine oil and coal tar to float Ag concentrate to

the surface of the flotation vats, enabling it to be scooped off and refined to Ag bullion or shipped off-site (Ried et al., 1923; Sprague & Vermaire, 2018). The relatively large grain size of the Cart Lake tailings enabled by the more efficient flotation separation process is important to the mobility of As species through decreasing the surface area of primary As minerals, reducing mineral alteration rates and contaminant mobilization compared to other finer-grained tailings (Bowell et al. 2014; Sprague and Vermaire 2018). Since the Silverfields Mill made use of flotation separation and shipped all ore concentrates off-site for refinement, the elevated Hg and CN^- concentrations found in some of the earlier generation tailings due to chemical extraction mineral processing are not found in the Cart Lake tailings.

1.5 Previous Studies of the Cobalt Area

A gradually increasing body of knowledge of mine tailings geochemistry has led to improvements in the understanding of the aqueous geochemical and mineralogical interactions taking place in many of the tailings deposits that affect the mobilization of toxic elements into nearby water systems.

Cart Lake, the research site for this project, has been included in several studies to date. However, it is one of the lesser studied lake-associated tailings deposits in the area, with the most heavily studied bodies being Crosswise, Peterson, and Cobalt Lake tailings. Previous research has been broad in geographic and scientific scope, with data from multiple tailings deposits and wetland systems and a variety of sample media. Cart Lake has been included in these studies (Clarke, 2017; Dumaresq, 2005; Dumaresq et. al., 2007, Sprague et. al., 2018; Michel et. al., 2007), but due to its lower groundwater As concentrations it has never been the sole subject of a research project.

1.5.1 Tailings Geochemistry and Mineralogy

The first extensive study of the aqueous geochemistry and mineralogy of the tailings in the CMC was carried out by Charles Dumaresq in 1993. This study investigated the transport and mobility of As and the associated risk to the water supply of nearby Cobalt (Dumaresq 2005). Through laboratory analytical methods, it was shown that As in

Cart Lake mobilized at a rate of 15 mg/kg of tailings per year, although most of this mobilized As was subsequently fixed in secondary minerals (Dumaresq 2005).

Laboratory leachate experiments using samples from the Cart Lake tailings indicated that the majority of As is released via oxidative weathering of primary minerals and dissolution of secondary minerals, although it is estimated that due to the precipitation of secondary minerals, the quantities of As released into local groundwater may be less than observed in laboratory experiments (Dumaresq, 2005). The tailings in Cart Lake contained 0.21% As by weight, or 2100ppm (Dumaresq 2005). Dumaresq also used XRD to determine the mineralogical composition of the Cart Lake tailings, which limited the study to bulk mineralogy and may not have been sufficiently sensitive to detect and characterize the secondary minerals forming in the tailings. Using the aqueous geochemical modelling software WATEQ4F, it was estimated that all of the As being mobilized was in As^{5+} form, but the modelling software does not account for geomicrobial influences which could be expected to increase the proportion of As^{3+} in the tailings (Dumaresq 2005).

Percival et al. (2004) expanded upon previous tailings characterization work with further sampling and discussion targeting the mobility and transport of several elements including As, Co, and Ni in the Nipissing Low Grade (NLGM) and High-Grade (NHGM) sites, Cart, Crosswise, and Peterson Lakes, and Mill and Farr Creeks (Percival et al. 2007). Using a combination of X-ray fluorescence (XRF), ICP, and XRD, it was determined that these tailings are silicate-dominated (plagioclase, quartz, chlorite) with significant carbonates (calcite, dolomite) (Percival et al. 2007). Secondary As minerals such as erythrite and scorodite were found in all tailings deposits studied and several others in lesser abundance, resulting from transport of elements mobilized via weathering of these minerals (Percival et al. 2007). This study estimated a mean annual discharge of 10 000 kg As into Lake Timiskaming from the combined wetland system linking these tailings deposits (Percival et al. 2007).

Beauchemin and Kwong (2006) and Kwong et. al. (2007) used SEM, X-ray absorption spectroscopy (XAS), ICP-AES, and scaled laboratory redox experiments to characterize secondary minerals and analyze the influence of biogeochemical factors on

As speciation, mobility, and transport in the Farr Creek drainage system. This study found that the mobility of As was highly affected by changes in redox chemistry, with mobilization increasing in reducing conditions due to greater solubility and higher relative proportions of As^{3+} (Beauchemin and Kwong 2006). Increasing microbial activity via addition of glucose was found to impact dissolution and speciation of As, suggesting As geochemistry is biologically mediated (Beauchemin and Kwong 2006). Further supporting this trend, concentrations of dissolved As were greater in the lower layers of the sediment profile than the upper layers due to the increased solubility of the biologically reduced As^{3+} prevalent in those areas and lower counts of iron- and sulfate -reducing bacteria (Beauchemin and Kwong 2006). Kwong et. al (2007) used SEM to investigate primary and secondary mineralization and found that the tailings are a source rather than a sink of As to local hydrological and hydrogeological systems, Al oxides were the main attenuators for As concentrations due to a lack of As-precipitating Fe oxides, and that P was a major competitor for As absorption sites on these minerals (Kwong et al. 2007). These studies found that the principal secondary mineral phases exerting control on As mobilization were erythrite and minor annabergite in the unsaturated zones, and scorodite in the saturated and unsaturated zones (Kwong et al. 2007).

A 2017 Master's research project carried out by Jeff Clarke (M.Sc.) at Queens University characterized the Nipissing and Cart Lake tailings deposits in the CMC. This study found that Cart Lake had the lowest levels of As in the study (below 1000 ppm As in all solid samples), due to the higher efficiency of mineral separation technology implemented during the time the Silverfields Mill was in operation and the shipping of As-bearing concentrate off-site (Clarke 2017; Anderson 1993). The bulk composition of the Cart Lake tailings was found to be over 90% silicates, approximately 3% carbonates, and the remainder of unknown or varied composition. The distribution of primary (arsenide, sulfarsenide, sulfide) vs. secondary (arsenate, Fe-oxide, arsenolite) As phases was found to be almost equal, with percentages of 42% and 58% respectively (Clarke 2017). Arsenic-associated mineral phases identified include Fe oxides, arsenates, arsenides, sulpharsenides, sulfides, and arsenolite (Clarke 2017).

1.5.2 Surface Water and Groundwater Compositions

Several studies have included surface water and groundwater sampling programs in the Cart Lake area (Clarke, 2017; Dumaresq, 2005; Percival et. al., 2007; Sprague and Vermaire, 2018). Surface water studies tend to lump together Peterson Lake and Cart Lake (Figure 2), as the two are hydraulically connected by a thin stream and wetland system that flows northward between the two systems. However, the tailings in each have different compositions, being from different eras of ore refinement, and each merit their own classification and analysis.

Outflow from Cart Lake into the wetland between Cart and Peterson lakes showed elevated As concentrations (1.160 to 1.800 ppm), but the flow from the wetland into Peterson lake showed reduced concentrations (0.070 to 1.090 ppm) (Dumaresq 2005). This may indicate the precipitation of As in the Cart Lake outflow by the wetland. The As concentrations in Peterson Lake, however, are higher than Cart Lake due to the influence of the Nova Scotia tailings in the eastern lobe of Peterson Lake (0.406 to 4.050 ppm) (Dumaresq 2005).

Another study in the nearby Farr Creek drainage system reported concentrations of As, Cu, and Zn consistently above the CCME water quality guidelines for freshwater aquatic life (0.005 ppm As, 0.002 ppm Cu, and 0.03 ppm Zn), sometimes by orders of magnitude (Kelly et. al., 2007). These findings are corroborated by multiple other studies, but few of these studies focus on Cart Lake (Kwong et al. 2007; Percival et al. 2007; Sprague et. al., 2016;).

By far, the most extensive groundwater sampling program at Cart Lake was carried out by Charles Dumaresq in 1993. Thirty-five piezometers were installed at strategic points throughout the tailings, to attempt to capture the spatial variability of the groundwater geochemistry. A summary of several key geochemical parameters from the initial sampling of these piezometers are in Table 2.

Table 2 - Results of Cart Lake key geochemistry parameters (Dumaresq, 2005)

	pH	Eh (mV)	Alkalinity (mg/L CaCO3	Conductivity (mS/cm)	Temperature (ºC)
Number of samples	33	12	31	32	13
Mean	8.0	252	190	680	6
Standard deviation	0.9	16	65	191	3
Minimum	7.1	229	105	310	1.0
Maximum	9.7	287	365	1030	13.0

The sampling program used bailers to extract water samples from the piezometers, and the samples were stored in clean glass apple juice containers for 12 hours before being transferred to polyethylene bottles. Due to the disruptive nature of bailer sampling, it is possible that oxygen was introduced into these groundwater samples, modifying properties such as the Eh, pH, and alkalinity.

Charles Dumaresq's study inferred that groundwater flows to the north-north-west (NNW) due to the topographic gradient (Dumaresq, 2005).

Appendix 2 shows the locations of Charles Dumaresq's piezometers. This map was modified from its original version, through georeferencing with current aerial photos of the lake. Many of these piezometers were found to be missing or broken and could not be sampled as a part of this project.

Story Environmental has nested piezometer installed near the sites of vertical core extraction, but the deepest piezometer in this nest is screened well below the bottom of the tailings and was not monitored as a part of the current study.

1.5.3 Cart Lake Revegetation Projects

Cart Lake is one of the only tailings sites in the CMC to be the site of revegetation campaigns, although other tailings deposits have been naturally revegetated to varying extents. Revegetation was carried out on Cart Lake to limit windblown dispersion of tailings in the area. Reports pertaining to the revegetation of Cart Lake could not be found, but other studies of naturally revegetated tailings in the area found that *Juncus balticus* and *Equisetum pratense* were the main species present, and that the toxic properties of the tailings inhibited biodiversity (Michel and Henein 2007).

In 1979, a research firm based out of Guelph, ON (Mine Waste Reclamation) carried out a revegetation study spanning 13 plots on the Cart Lake tailings, with various seed types, fertilizers, and topsoils. The original reports are located in the Cobalt Resident Geologist's files and could not be accessed prior to the writing of this thesis. However, Anderson (1993) summarizes the report. The experiment showed a good degree of success, with the majority of the plots still vegetated in 1984. However, test plots have been slowly decreasing in area as windblown tailings encroach upon and burying the vegetation. The large particle size and resulting well-drained nature of the tailings create a dry surface in the unvegetated state, but areas that were used as test plots in the revegetation study have begun to develop soil horizons. (Sprague and Vermaire 2018). An analysis of these horizons carried out by Charles Dumaresq in 1993 showed As concentrations ranging from 305 ppm to 1150 ppm, and varying, but generally low, concentrations of other toxic elements such as mercury (Dumaresq 2005). Table 2 and Figure 3 are excerpts from Dumaresq (2005) showing trace element concentrations and developed soil horizons on one of the former revegetation plots.

Table 3 - Trace element concentrations from Cart Lake soil horizons (excerpt from Dumaresq, 2005)

Element	Cart Lake Soil – "A"	Cart Lake Soil – "E"	Cart Lake Soil – "B"	Cart Lake Soil – "C"	Cart Lake Crust #2
Al (%)	2.14	3.66	1.19	1.83	3.14
Fe (%)	4.57	7.51	1.78	3.84	6.25
Mg (%)	4.3	5.91	1.42	3.92	5.73
Ca (%)	0.8	1.25	0.3	1.2	1.67
Na (%)	0.02	0.04	0.02	0.04	0.04
K (%)	0.09	0.2	0.04	0.06	0.1
As (ppm)	518	1150	305	660	696
Sb (ppm)	9.6	14.8	3.1	9.2	169
Mn (ppm)	675	1048	275	661	978
Cl (ppm)	2.08	6.36	4.17	0.16	0.48
SO4 (ppm)	6.1	40	10.7	24	44
Hg (ppm)	8	17	4	5	15
Cu (ppm)	57	174	12	82	221
Pb (ppm)	163	178	15	184	281
Zn (ppm)	175	188	37	180	298
Mo (ppm)	3	2	3	3	4
Co (ppm)	253	489	19	146	534
Ni (ppm)	125	289	37	82	397
Cd (ppm)	<0.2	<0.2	0.2	<0.2	<0.2
Cr (ppm)	113	158	42	97	160
Bi (ppm)	21	55	6	15	31
Ba (ppm)	11	25	24	8	20
V (ppm)	111	180	36	96	159
Sr (ppm)	7	9	12	6	21
Y (ppm)	6	12	2	4	10
Sc (ppm)	10	17	<5	8	15
Ag (ppm)	16.6	32.2	2.2	12.5	71

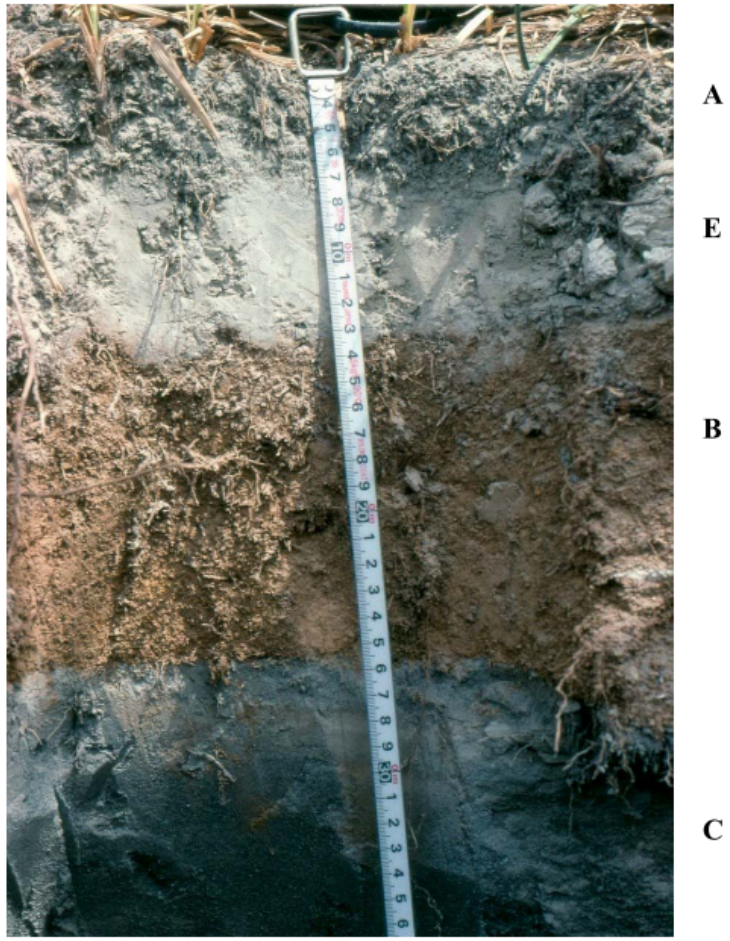

Figure 3 - Soil horizons developing on Cart Lake years after revegetation (Dumaresq, 2005)

1.6 Literature Review Summary – Gaps in Knowledge

Cart Lake has been included in many studies to date, but as of yet has not been the sole subject of a research project. Its mineralogy and groundwater chemistry are fairly well understood, but a lack of a robust interpretation of the geochemical interactions between the pore water, tailings particles, and microbial community is apparent.

Previous groundwater studies of Cart Lake employed bailers to extract samples from piezometers. The EPA recommends against the use of bailers in sampling programs such as these as they have a tendency to aerate the sample and mix aquifer representative water located in screened well sections with stagnated water above the screen, modifying key geochemical parameters. Collection of water samples via low-flow methodology, and in-field anaerobic measurement of certain parameters, enables a more accurate measurement of pH, Eh, and alkalinity, all of which are highly important in the control of element mobilization.

Prior to the present study, no high-resolution sampling had been conducted at Cart Lake to analyze the changes in cation and anion concentrations along a vertical profile, useful in the derivation of conclusions regarding contaminant mobility and zonation. A nested piezometer, installed by the consulting firm Story Environmental, has one screened section in the tailings and another below the bottom of the lakebed sediments, but none in between.

Most primary minerals and generic secondary mineral families found in the Cart Lake tailings have been fairly well characterized. However, a lack of information pertaining to specific secondary mineral phases has been observed. Specific Ca-Fe mineral phases such as yukonite and arseniosiderite have been hypothesized to exists in the tailings, but have not been positively identified (Clarke, 2017).

Geochemical modelling packages such as PHREEQC are useful in speciation calculations, saturation index determination, and reactive transport modelling. Elemental concentration data collected along a vertical pore water profile can be analyzed in conjunction with secondary mineral coatings to inform discussion on the controls on transport of As and other contaminants through the tailings porewater.

Little, if any, geomicrobial work has been carried out on these tailings. The importance of microbes in redox chemistry and element mobilization is well documented and understood, and the incorporation of microbial considerations furthers our understanding of the toxicological properties of these tailings.

A comprehensive discussion of liberation, transport and attenuation processes affecting toxic As species has yet to be carried out on the Cart Lake tailings. In order to effectively analyze these processes, data collection from one location along a vertical pore water profile will be furthered by modelling using the PHREEQC software package, with additional discussion on the significant role of As-utilizing microorganisms that may be present on site.

1.7 Objectives and Scope

The primary objectives of this research project were to:

1. Collect and analyze porewater samples from piezometers in the Cart Lake tailings and from tailings cores collected along a detailed vertical profile through the vadose zone.
2. Determine the primary and secondary mineralogy of the tailings particles through analysis of thin sections, with a focus on oxidative weathering of primary ore minerals and characterization of the resulting secondary minerals.
3. Interpret and discuss mineralogical and aqueous geochemical data to determine the geochemical processes controlling As mobilization, transport and attenuation.
4. Provide recommendations for future research work to be carried out on site.

1.8 Hypotheses

Based on previous studies of the Cobalt area and aqueous geochemical and mineralogical studies in similar environments, the following controls on As mobilization, transportation, and attenuation are expected to dominate in the Cart Lake tailings:

- The pH of the tailings will be neutral to slightly basic, due to the high concentration of buffering carbonate minerals present in the Cart Lake tailings. This will reduce the rate of toxic element mobilization.
- Oxidative dissolution of members of the skutterudite solid solution series (skutterudite, nickelskutterudite, ferroskutterudite), arsenopyrite, and other reactive sulphide and arsenide minerals will be the primary sources of As in the pore waters
- Most As will be present in As^{5+} in the Cart lake tailings pore water
- Co-precipitation and sorption of As with Fe-oxyhydroxides will be a strong control on As attenuation through the water column.
- Most As will be transported as As^{5+}.
- Formation of secondary mineral coatings around primary grains will remove As from solution, although As may be remobilized from these coatings where geochemical conditions allow. The dominant secondary mineral phases are expected to be scorodite, erythrite, and Fe-Ca arsenates such as yukonite and arseniosiderite
- Geomicrobial activity is expected to be a strong control on all As mobilization and attenuation, although this will prove difficult to characterize.

2 Methods

2.1 Field Methods

Sample collection was carried out at Cart Lake from October 14 to 17, 2019. During this visit, the following samples were collected:

- Groundwater from existing piezometers (6 samples), for aqueous geochemical analysis
- Three vertical cores to a depth of 2.66 m bgs, for mineralogical and pore water aqueous geochemical analysis in the vadose and saturated zones
- Horizontal cores collected from the side of a test pit to a depth of 1.0 m, at 0.10 m intervals, for higher resolution pore water aqueous geochemical analysis in the vadose zone

2.1.1 Groundwater Sampling

2.1.1.1 *Equipment Preparation*

All water sample containers were filled with DI water, left to sit for a minimum of 2 days, then emptied and filled with DI water again for a minimum of 2 soak cycles. The bottles in which the cation samples were collected (60 mL Nalgene bottles) were further soaked in an acid bath for 4 hours containing 5% HNO_3, rinsed thoroughly, and then left in a DI water bath for a minimum of two days. Preservative acid (concentrated HNO_3, trace metal grade) was decanted into a small dropper for transport to the field. The same acid dropper was also used to create field blanks run concurrently during sample analysis.

Using well depth information from previous reports, 4 m lengths of new, clean 1/8” ID High Density Polyethylene (HDPE) tubing were prepared with luer lock adapters for piezometer sampling and packaged in sealed bags for transport.

Thermo Fisher Scientific pH and Ag-AgCl combination redox probes, pH/redox meters (JJS Jenco MODEL-5005, Barnant 20) and Ross filling solutions were used for in-field analysis (Table 4).

Table 4 - pH and Redox Probe and Solution Details

pH	Electrode Make	Thermo Fisher Scientific
	Electrode Model	ROSS Comb. pH Electrode Epoxy Body, Lot Code UW1
	Filling Solution	ROSS Thermo-Fisher Reference Electrode Filling Solution - Orion 810007, Lot WY1
Redox	Electrode Make	Thermo-Fisher Scientific
	Electrode Model	Orion Sure-Flow Combination Redox Electrode
	Filling Solution	Thermo Fisher Orion 900011

Combinations of various pH electrodes and meters were tested by carrying out two-point (7, 10) calibrations, with linearity check at pH 4 using pH buffer solutions. Combination redox probes and meters were tested by checking redox potential values (mV) when the probe was immersed in freshly prepared Zobell's solution.

Verification of the HACH digital titrator used for in-field alkalinity titrations was carried out and the volume of titrant per unit dispensed was found to align exactly with the HACH-advertised value (0.001263 mL/unit). Bromocresol-green/Methyl-red indicator (BCG-MR) was used for all titrations carried out over the course of this project. The titrant used was H_2SO_4 in concentrations of 1.6 N and 0.16 N depending on expected alkalinity values.

2.1.1.2 *Groundwater Sampling and In-Field Analyses*

Sampling of existing piezometers was carried out on October 15, 2019. The location of all sampled piezometers is shown in Figure 4.

All pre-existing piezometers were located and assessed for physical condition. At each location, GPS coordinates were collected and depth to water (DTW) and stickup (St) were recorded using a Heron Skinny Dipper water level sounder (WLS) and a small tape measure.

Six groundwater samples (Table 5; Fig. 4) were collected from piezometers previously installed by Dumaresq (2005). Piezometers CL-17S and CL-17D, being nested piezometers, have the same geographic coordinates.

Table 5 - Piezometer IDs and geographic coordinates

Project ID	Dumaresq (2005) ID	Northing	Easting
CL-6	6	47.37853	-79.68606

Project ID	Dumaresq (2005) ID	Northing	Easting
CL-8	8	47.37927	-79.68553
CL-17S	17	47.37902	-79.68502
CL-17D	17	47.37902	-79.68502
CL-18	18	47.37881	-79.68453
CL-27	27	47.37827	-79.68560

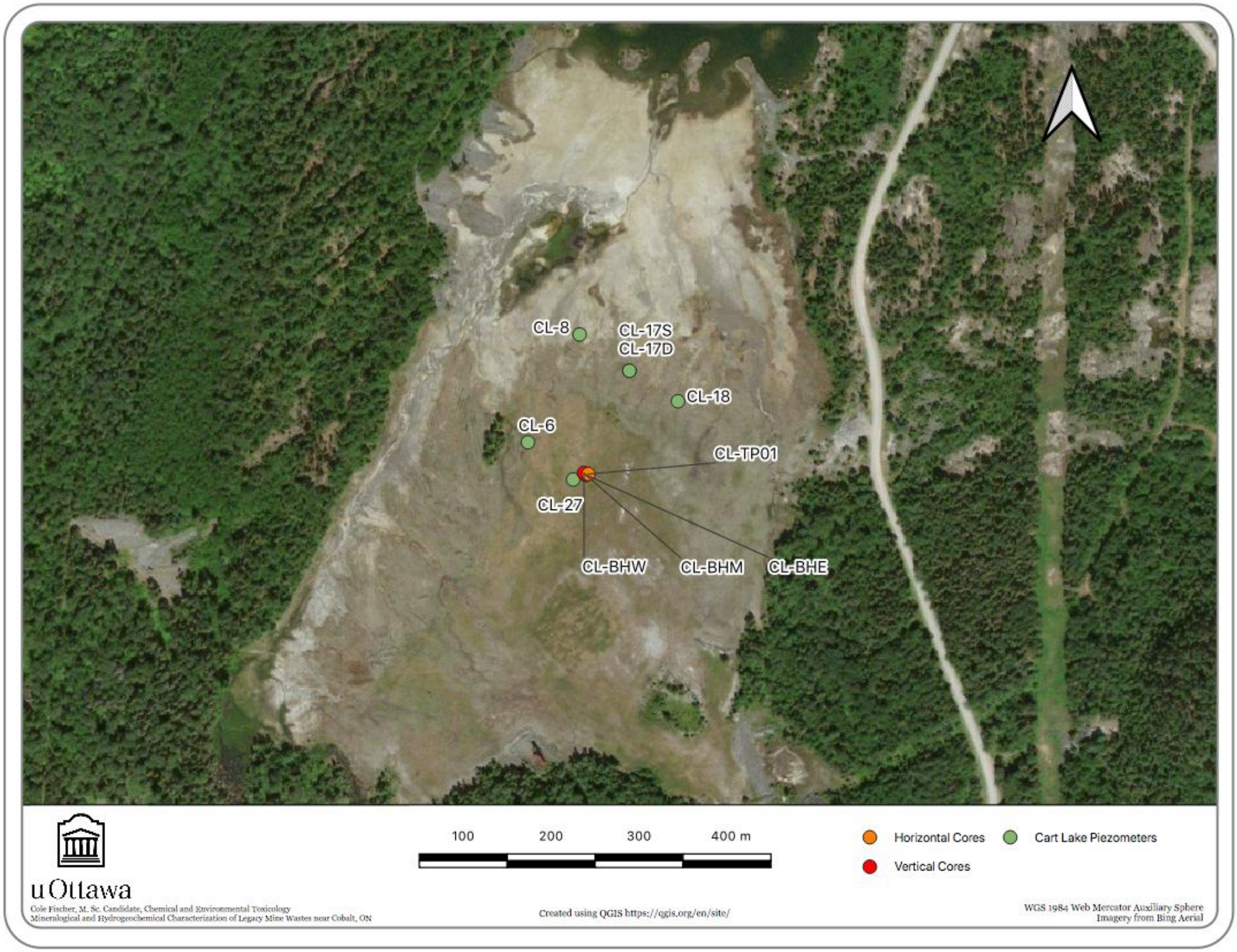

Figure 4 - Cart Lake piezometer, borehole, and test pit locations

HDPE tubing sections were deployed as near as possible to the bottom of the piezometers, based on borehole installation information (Dumaresq, 2005). A minimum of five syringe volumes (300 mL) were removed and purged to the ground, then three new, clean 60 mL syringes were filled, from which samples were collected and parameters measured.

A custom-made flow-through cell was used to measure pH and redox potential while expressing the volume of an entire syringe through the cell at a rate of approximately 12 mL/min, to reduce exposure to atmospheric oxygen. The redox vales were corrected to the Standard Hydrogen Electrode (SHE) using the reference potential for the electrode (+208 mv) determined from the known Eh for Zobell's solution (Nordstrom, 1977).

Alkalinity was measured using a HACH digital titrator with BCG-MR indicator on 30 mL volumes of filtered (0.45 μm) sample. The calculation endpoint was determined to be reached at the instant when the sample changed from violet to light pink, but several intermediary colour changes were recorded as well (blue-grey, grey, violet). Each titration was carried out in duplicate and the results were averaged.

Samples for cation (45 mL) and anion (20 mL) analysis were filtered 0.45 μm into pre-cleaned 60 mL HDPE containers. Samples for anion analysis were left unpreserved and samples for cation analysis were preserved using concentrated HNO_3 to a pH of <2.

All water samples were immediately placed into a cooler with ice packs and transferred to the fridge upon return, within 6 hours of collection.

2.1.2 Vertical and Horizontal Tailings Cores

Vertical and horizontal tailings cores were collected near the center of the tailings impoundment as shown in Figure 4. The cores were used for mineralogical investigation and for extraction and analysis of pore water to generate a vertical aqueous geochemical profile. The horizontal cores were collected to provide relatively high resolution data in the unsaturated zone (above ~1.6 m bgs based on GW levels of the nearest piezometer, CL-6).

2.1.2.1 *Equipment Preparation*

A Pionjar gas-powered drill was used for vertical coring with a custom-fabricated drive head. Core catchers were fitted to the bottom of three 3 m lengths of 5 cm diameter aluminum tubes for the vertical core extraction. Caps for all core sections were punctured to prevent pressurization during placement, and sealed with electrical tape once in place.

2.1.2.2 *Vertical Core Extraction*

Three vertical ~3 m cores were collected 0.5 m apart to depths of 2.66 m, 2.56 m, and 2.59 m bgs respectively at the location shown in Figure 4, (BH-East (CL-BHE), BH-Middle (CL-BHM), BH-West (CL-BHW)).

A chain lift was used to extract the aluminum tubing from the tailings. A pipe cutter was used to divide the core into 50-60 cm sections for mineralogical investigations (CL-BHE/BHM) or 20 cm sections for pore water extractions (CL-BHW). Sections were capped, sealed with tape, and labelled with a vertical-up direction indicator.

Compression of the tailings occurred during collection of the vertical cores due to friction inside the core tube and the unconsolidated nature of the tailings. Compression compensation factors were calculated for each core by dividing penetration depth by the length of the final recovered core. These factors were used to correct measurements on the cores to the actual depths.

2.1.2.3 *Horizontal Core Extraction*

A test pit was dug adjacent to the locations of the vertical cores to a depth of 1.1 m bgs. Ten 20 cm sections of aluminum tubing were hand-pressed into the side wall of the test pit at 0.1 m vertical intervals, then capped, extracted, and sealed. Samples were labelled using the convention CL-TP0xx, with the xx representing the depth in m bgs.

2.2 Thin Section Preparation

Two of the vertical cores (CL-BHM, CL-BHE) were bisected lengthwise, photographed, transferred to a drying box, and dried anaerobically in preparation for mineralogical analysis. The core drying box was sealed and connected with polyethylene

tubing to a desiccant column in a closed loop containing N_2 gas circulated with a pump. Desiccant was changed as necessary according to the colour indicator, and the system was flushed with new N_2 gas for a minimum of 15 minutes after desiccant changes. The cores were determined to be sufficiently dry when the desiccant indicator did not change over two days.

Twelve locations on the cores were chosen for preparation of polished thin sections based on colour, and grain size, with several locations selected above and below fine-grained layers that may have acted as O_2 diffusion barriers. Sample identification information with sample depths is presented in Table 6.

Sample ID	Sample Depth (m bgs)
TS-1	21.2
TS-2	33.9
TS-3	53.0
TS-4	80.6
TS-5	91.2
TS-6	108.1
TS-7	120.8
TS-8	146.3
TS-9	159.0
TS-10	178.1
TS-11	188.7
TS-12	201.4

Table 6 - Thin Section Sample Depths

A two-part low-viscosity epoxy resin (EPO-TEK 301-2FL) was applied to the core surface using a dropper until the surface began to appear slightly saturated and left to harden overnight. After the first application of epoxy had cured, the segments of interest were removed from the core tube and fully immersed in epoxy under vacuum to fully embed the material prior to preparation of thin sections. The embedded segments were shipped to the Earth Science Department at the University of New Brunswick (UNB) for preparation of polished thin sections.

All thin sections were oriented parallel to the core axis and therefore perpendicular to bedding layers in the tailings. The sections were cut and polished for a final thickness of 100 μm.

2.3 Pore Water Extractions

Pore water was extracted using a centrifuge, centrifuge tube, and a centrifuge tube insert machined from Delrin plastic (Figure 5). Sediment was extracted from the core segments in multiple ~20 g subsamples in an anaerobic chamber, packed into the centrifuge tube inserts, covered with parafilm to prevent oxygen ingress, and centrifuged. All samples were spun at 5000 rpm for 20 minutes, including spin up and spin down. Filter paper, cut to the exact size of the bottom of the centrifuge tube insert, prevented sediment from being pushed into the extracted pore water in the centrifuge tube.

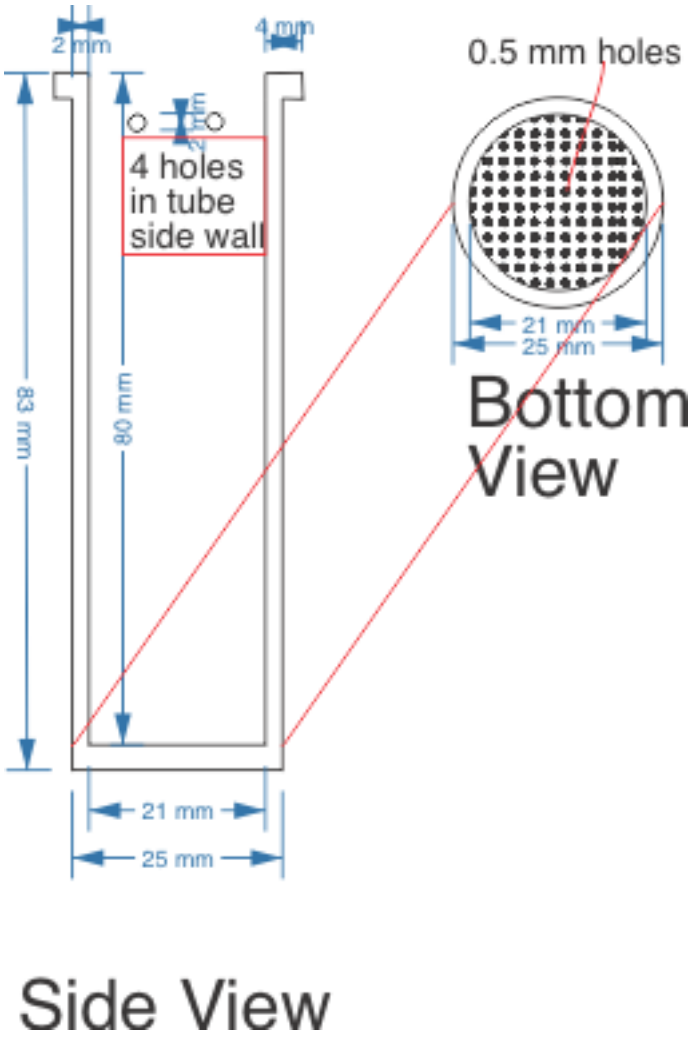

Figure 5 - Centrifuge tube insert used to extract pore water from sediment samples

Extracted pore water was filtered using 0.2 µm MinisartNML Plus Hydrophilic filters into clean 15 mL falcon tubes. Employing methodology similar to that used for the field analyses, pH, redox potential and alkalinity were measured immediately from 5, 5, and 10 mL subsamples respectively. The remaining sample volume was divided into previously cleaned 15 mL falcon tubes and preserved for cation and anion analysis as described above.

2.4 Analysis Methods – Water Samples

All water samples were analyzed using a combination of Inductively Coupled Plasma (ICP) - Mass Spectroscopy (MS), Optical Emission Spectroscopy (OES), and Ion Chromatography (IC). The constituents analyzed using each method are outlined in Table 7 below.

Table 7 - Aqueous ion analytes for groundwater and extracted pore water analysis

	ICP-OES	ICP-MS	IC
Analytes	Majors ● Ca ● Mg ● Na ● K Minors ● Fe ● Si ● Mn ● Sr ● Ba ● Al ● S	Minors ● Fe ● Mn ● Sr ● Ba ● Al ● As Traces ● Sb ● Co ● Cu ● Pb ● Zn ● Ni ● Cd ● Ag ● Sb ● Mo	Majors ● SO4 ● Cl ● F ● NO3 ● PO4

For samples from core sections that yielded insufficient volume, dilutions were carried out using DI water for IC samples, and 5% HNO_3 (Trace Metal grade) for ICP-MS and ICP-OES.

Accuracy and precision were estimated by analyzing data from certified reference solutions and calibration standards respectively. Accuracy was determined by dividing the average concentrations of all measurements of each analyte in the certified reference standard by their respective known reference values. Precision was estimated by calculating the relative standard deviation for three replicate analyses of a calibration solution, with 0% representing perfect precision.

Limits of detection (LOD) were determined individually for each element, using the generally accepted formula of 3x the standard deviation for analyte concentrations in blanks.

Variance was calculated by averaging squared differences from the mean for each parameter.

2.5 Analysis Methods - Thin Section Mineralogy

Thin sections were examined using a petrographic microscope to identify regions of interest (ROI) for further detailed analysis with scanning electron microscopy (SEM)/ Energy Dispersive Spectroscopy (EDS) and electron microprobe analysis (EMPA). Several ROIs were selected from each section, based on distinctive coloration, reflectivity, and occurrence of primary reactive sulf-arsenide minerals and associated alteration products.

2.5.1 SEM-EDS Analysis

All thin sections were carbon coated prior to SEM and EPMA analysis. Analyses were conducted using a JEOL 6610LV SEM equipped with an Oxford INCA large area SDD detector for EDS analysis. The SEM/EDS analyses were conducted using a beam accelerating voltage of 20 kV. Thin sections were scanned for sites of interest at low magnification, then EDS spectra and images were acquired at higher magnifications. From these images, primary reactive minerals and alteration products were identified and EDS spectra were collected and recorded for both primary and secondary phases.

The EDS data were exported to Desk Top Spectrum Analyzer II (DTSA-II) (*NIST Desktop Spectrum Analyzer II*, 2021). Relative elemental peak heights were viewed in the software to further identify and differentiate primary and secondary minerals.

Mineral compositional information from mindat.org was compared to EDS spectral data to identify primary and secondary minerals present in the thin sections.

2.5.2 EMPA Analysis

The EMPA analyses were carried out using the JEOL 8230 SuperProbe in the University of Ottawa microanalysis lab. Compositional analyses were acquired using five

tunable wavelength dispersive spectrometers (WDS). Calculations of atomic percentages for primary and secondary minerals were completed based on the expected mineral composition (i.e., sulfide/arsenide or oxide phases). Standards of known composition were used during all EMPA analyses, presented in Appendix 3.

Analyses were conducted at discrete points, along one-dimensional traverses, and in two-dimensional maps for primary sulfide/arsenide and secondary oxide minerals. Different EMPA operating conditions were employed in each case as shown in Table 8.

Table 8 - EMPA Operating Conditions

Operating Condition	Arsenates	Sulfides/Arsenides
Takeoff angle	40º	40º
Acceleration voltage	15 keV	20 keV
Beam current	20 nA	40 nA
Beam diameter	2 microns	1 micron

The point analyses, traverses, and maps were collected in areas where primary minerals were observed to have weathered to secondary minerals. Efforts were made to analyze discrete, homogeneous mineral phases and avoid mixed assemblages. Traverses of ~20 μm were collected in primary mineral alteration zones, alongside analytical maps of alteration areas.

3 Results

3.1 Cart Lake Groundwater Geochemistry

3.1.1 Piezometer Sampling Results

A summary of pH, Eh, and alkalinity measurements collected from sampled piezometers is presented in Table 8.

Table 8 – Alkalinity, pH, and Eh measurements collected during water sample analysis

Piezometer ID	Alkalinity (mg/L HCO_3^-)	pH	Eh (mV)
CL-6	182.94	7.96	209.2
CL-8	202.00	7.75	128.0
CL-17S	148.64	7.78	46.0
CL-17D	45.74	7.22	100.0
CL-18	117.20	7.60	207.2
CL-27	91.47	6.75	157.0
Max	202.00	7.96	209.2
Min	45.74	6.75	46.0
Mean	131.33	7.51	141.2
St. Dev.	58.43	0.45	63.5

The pH of all piezometer samples is circumneutral to slightly basic (6.75 to 7.96). The Eh ranges between 46.0 to 209.2 mV, and alkalinity ranges between 45.74 and 202.00 mg/L HCO_3^-.

The principal cationic species observed in the piezometer samples are Ca (4.85 mg/L-75.305 mg/L), Na (2.09 mg/L-8.75 mg/L), Mg (1.25 mg/L-6.70 mg/L), and K (1.13 mg/L-3.51 mg/L). Silver and Cd are below detection limits for all samples except for one (CL-18), both with concentrations less than 0.001 mg/L. Concentrations of Co, Mo, Sb, Pb, and Zn are also below instrument detection limits at CL-17S and CL-27, and in concentrations near the detection limits at the other piezometers. The range in concentrations for Ca (817.40) and As (45.30) were the highest of all cations.

The principal anionic species present in these groundwater samples are oxyanions of As (0.003 mg/L-15.51 mg/L), HCO_3^- (45.73 mg/L-201.99 mg/L), SO_4^{2-} (6.81 mg/L-83.56 mg/L), and PO_4^{3-} (0.044 mg/L-9.63 mg/L). Concentrations of Cl^- (0.35 mg/L-4.08 mg/L),

F^- (0.06 mg/L-0.24 mg/) and NO_3^- (0.19 mg/L-2.53 mg/L) are above instrument detection limits at all piezometers. The ranges in concentrations of alkalinity (3414.47), SO_4 (1247.63), and PO_4 (15.15) concentrations are the highest of all analyzed anions. Arsenic is present in elevated concentrations in four samples (0.14 mg/L-15.50 mg/L), in trace concentrations in one sample, and was below instrument detection limits for one sample. No anions were observed below the detection limits of IC. No clear spatial trend was observed in cation or anion concentrations across the site.

The range of values and mean concentrations for detectable analytes are presented in Appendix 3 and Figure 6, where points represent sample means and the bars represent the range (max and min).

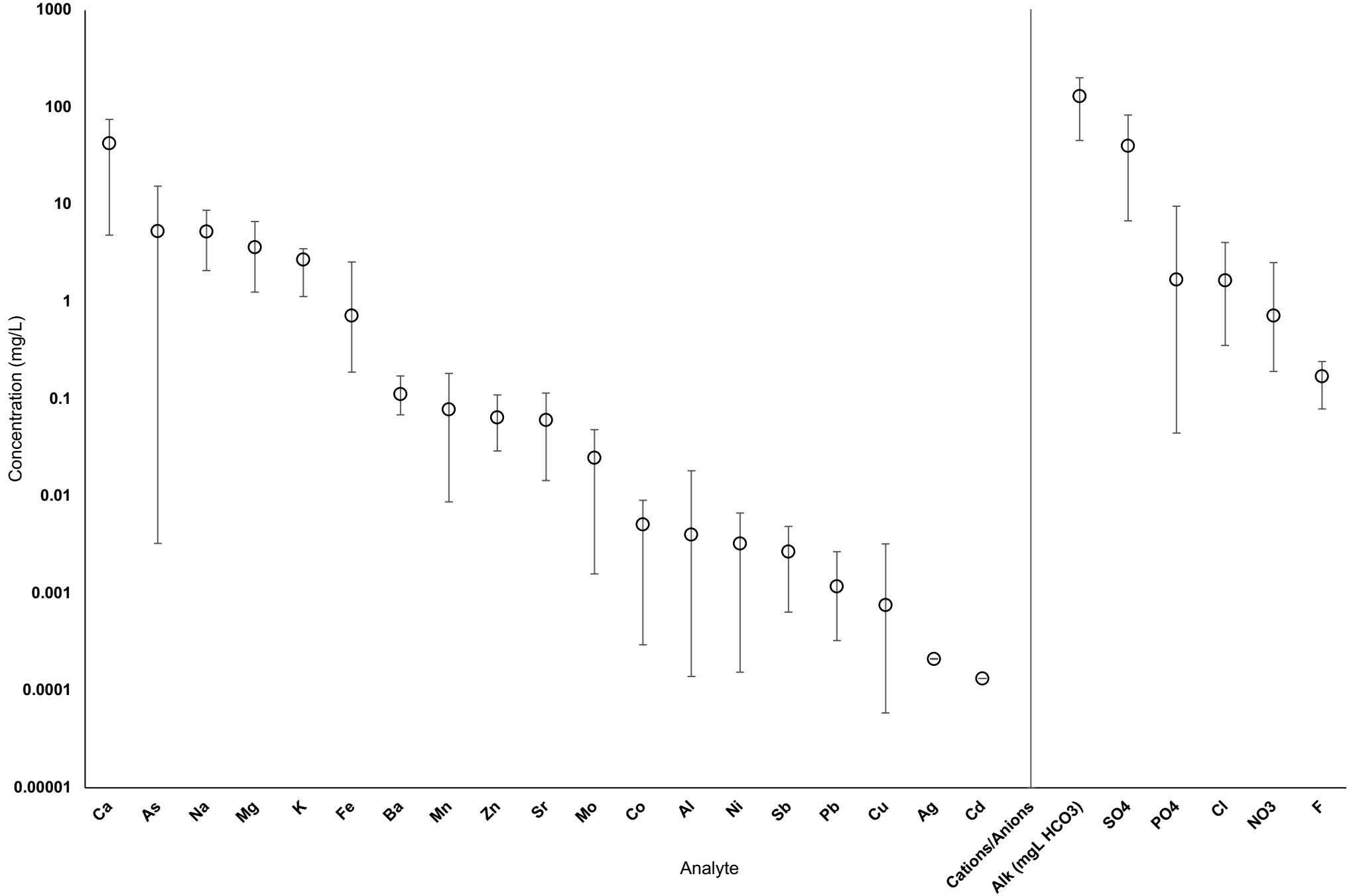

Figure 6 - Range in analyte concentrations from Cart Lake piezometer samples. Note logarithmic Y-axis scale.

3.2 Pore Water Sampling Results and Vertical Profile Analysis

A total of 16 water samples (10 from vertical core sections and 6 from horizontal cores) were extracted and analyzed as per the methods outlined in sections 2.3 and 2.4.

3.2.1 Geochemical Vertical Profiles

Geochemical profiles of key parameters pH, Eh, and alkalinity are presented in Figure 6 and Table 9.

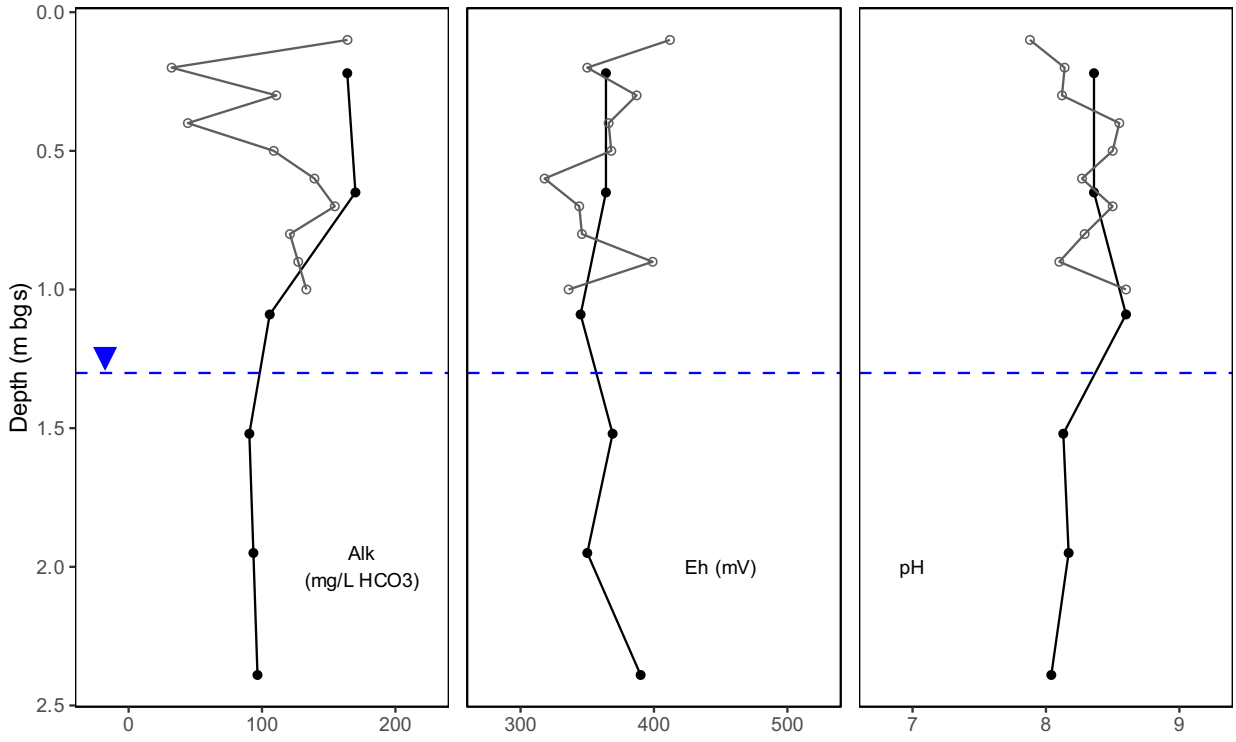

Figure 7 - Vertical profiles showing pH, Eh, and Alkalinity. Hollow points represent horizontal cores and solid points represent vertical cores Water level is indicated by the inverted blue triangle.

The pH values measured throughout the profile are circumneutral to slightly basic (7.88 – 8.6) and show a weak decreasing trend with depth save for an increase to the highest pH values observed in the profile (8.6) at a depth of 1.08 m bgs, just above the water table. Redox potential values do not show any observable trend with depth and vary between 318 and 412 mV. The highest Eh value is observed in the deepest sample extracted from the vertical core, at 2.39 m bgs. Alkalinity values vary between 0 and 200 mg/L HCO_3^- with no observable trend from surface to the water table, then remain

relatively constant near 100 mg/L HCO_3^- throughout the saturated zone. The results of field parameter analysis for the vertical profile are presented in Table 9.

Table 9 - Vertical Pore Water Profile Field Parameter Results

Sample source	Depth (m bgs)	pH	Eh	Alkalinity (mg/L HCO_3^-)
Test pit	0.1	7.88	412	164.1
Test pit	0.2	8.14	350	32.2
Vertical core	0.2	8.36	364	163.9
Test pit	0.3	8.12	387	110.7
Test pit	0.4	8.55	366	44.4
Test pit	0.5	8.5	368	108.8
Test pit	0.6	8.27	318	139.3
Test pit	0.7	8.36	364	170.0
Test pit	0.7	8.5	344	154.6
Test pit	0.8	8.29	346	120.9
Test pit	0.9	8.1	399	127.1
Test pit	1.0	8.6	336	133.2
Vertical core	2.6	8.6	345	105.8
Vertical core	3.0	8.13	369	90.5
Vertical core	3.5	8.17	350	93.6
Vertical core	3.9	8.04	390	96.6
	Maximum	8.6	412.0	170.0
	Minimum	7.9	318.0	32.2
	Mean	8.3	363.0	116.0
	St. Dev.	0.2	24.7	39.9

3.2.2 Vertical Pore Water Profile Analytical Results

The principal cation species throughout the vertical profile are Ca (22.42 mg/L-192.04 mg/L), K (2.86 mg/L-13.51 mg/L), Mg (1.23 mg/L-8.67 mg/L), and Na (4.62 mg/L-16.86 mg/L). The principal anion species are alkalinity (32.32 mg/L HCO_3^--170.01 mg/L HCO_3^-), As (0.952 mg/L-18.09 mg/L), SO_4^{2-} (6.95 mg/L-456.12 mg/L), Cl^- (0.76 mg/L-17.779 mg/L), and NO_3^- (0.69 mg/L-185.66 mg/L). Vertical pore water profile plots showing field parameters, anions, major cations, minor cations, and trace cations are presented in Figure 7 and Appendix 3.

Concentrations of major cations Ca, Mg, and Na increase to their highest values in the profile at approximately 2 m bgs. Concentrations of minor and trace cations Cd, Co,

Mn, Sr, and Zn show the same trend as major cations Ca, Mg, and Na. Concentrations of these trace and minor cations are less than 1 mg/L..

Sulfate concentrations increase by approximately 8x between depths 1.09 and 1.52 (from 26.55 to 217.41 mg/L), likely coinciding with the water table. Sulfate values increase (217 – 456 mg/L) near the bottom of the vertical profile but decrease to below 100 mg/L at the deepest point in the profile.

The lowest dissolved As concentrations in the vertical profile are observed near the surface where oxygen infiltration is greatest. Concentrations of As released via oxidation from primary reactive minerals and likely mobilized principally in pentavalent hydrogen arsenate form ($HAsO_4^{2-}$), increase to their highest values (19.09 mg/L) in the lower reaches of the vadose zone. A decrease from 15.98 mg/L to 7.00 mg/L occurs between 1.09 m bgs and 1.52 m bgs, coinciding with the water table at ~1.39 m bgs. Once below the water table, concentrations increase gradually to 10.96 mg/L at the deepest location analyzed in the vertical profile.

Several analytes were below the analysis detection limits (BD) at most depths, including Ag (BD at 9 out of sixteen measurements) and PO_4 (BD at 11 out of 18 measurements).

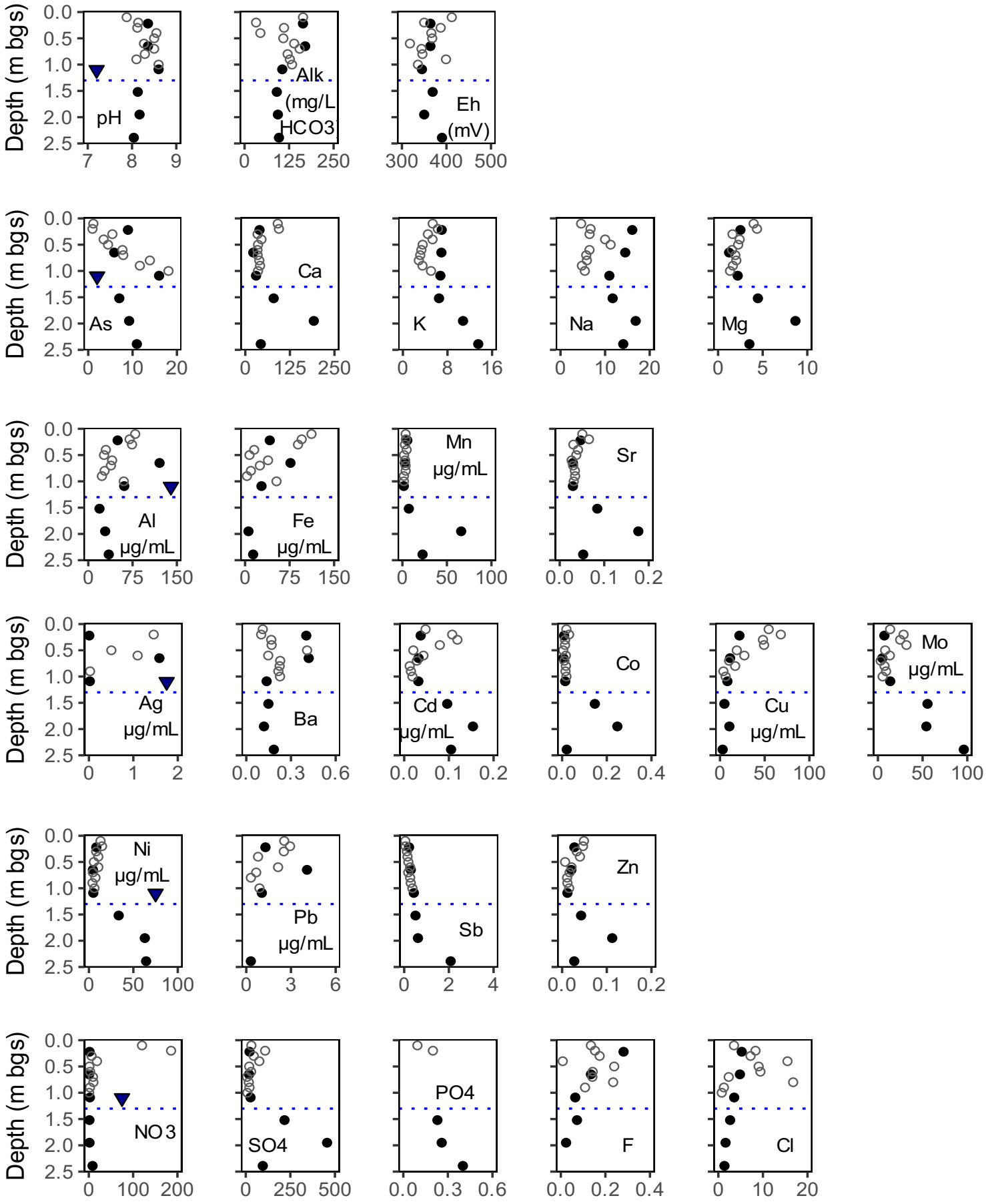

Figure 8 - Vertical pore water profile geochemical data. All concentrations are in mg/L unless otherwise indicated. Hollow grey circles represent sample points from the test pit, and solid black circles represent those from the vertical core.

3.3 Aqueous Ion Analysis QA/QC

3.3.1 Piezometer Samples

For ICP-OES and ICP-MS analyses, measurements of certified reference solutions to determine accuracy were not conducted for piezometer samples.–A preliminary estimation of accuracy, calculated from calibration solutions created specifically for these analyses, is provided instead. Precision is reported as the relative standard deviation for three replicate analyses of a calibration solution, with 0% representing perfect precision. It ranges between 0-18% respectively for all analytes, with a mean precision of 5%.

For IC, all samples were diluted by a factor of 5 using DI water. Blanks run concurrently during analysis consisted of DI water from the same source, prepared at the same time as the samples. Since no certified reference solutions were run during IC analysis, a calibration standard was run four times to analyze precision, which ranges between 0.2%-3.9%.

The results of piezometer QA/QC analyses are presented in Table 10. All samples were analyzed in the same ICP-MS/OES/IC runs.

Table 10 - Piezometer sampling QA/QC results

Method	Analyte	Accuracy (%)[1]	Precision (%)
ICP-OES	Al	97	3
	Ba	99	0
	Ca	101	2
	Fe	100	0
	K	98	2
	Mg	104	-
	Mn	98	2
	Na	99	1
	S	114	18
	Sr	99	1
ICP-MS	As	100	8
	Ag	104	4
	Cd	100	5
	Co	105	9
	Cu	103	9
	Ni	100	10

	Mo	98	7
	Pb	103	1
	Sb	97	9
	Zn	100	7
IC	Cl	140	0.5
	F	116	0.5
	NO_3	89	1.5
	PO_4	120	3.9
	SO_4	102	0.2

[1]Accuracy calculated from calibration solution

Four samples are outside the optimal range for charge balance error (0 +/- 5%), CL-6 at -8.50%, CL-8 at 6.89%, CL-17D at 8.24%, and CL-27 at -42.29%. The cause of these discrepancies is not known but may be attributable to specific redox states influenced charge balance. For CBE calculations, As was included with the cations as it is expected to have a positive charge based on solution conditions.

3.3.2 Vertical Pore Water Profile

For ICP-OES analysis, accuracy based on the certified reference solutions ranges between 69.69%-115.95% (GW-HI) and 65.30%-129.02% (GW-LOW), for analytes present in concentrations above the LOD. Precision of the standard reference solution analysis ranges between 0%-2% for analytes present in concentrations above the LOD. Accuracy based on calibration standards ranges from 94.77%-102.34%. Precision of the calibration solutions ranges from 0%-5%.

For ICP-MS analysis, accuracy based on the certified reference solutions measurements ranges between 93.83%-117.25% (GW-HI) and 92.94%-117.32% (GW-LOW) for analytes present in concentrations above the LOD. Accuracy based on calibration standards run five times throughout analysis ranges from 88.87%-100.11% for analytes present in concentrations above the LOD. Precision for ICP-MS ranges between 0%-10% for the certified reference solutions, and 1%-4% for the calibration solutions.

Since no certified reference solutions were run during IC analysis, calibration Standard 5 was run four times to analyze accuracy and precision. Accuracy ranges between 89.80%-140.88% for all analytes, and precision ranged between 0%-4%.

The results of extracted pore water QA/QC analyses are presented in Table 11.

Table 11 - Extracted pore water sampling QA/QC results

Method	Analyte	Accuracy (%)[1]	Accuracy (%)[2]	Accuracy (%)[3]	Precision (%)
ICP-OES	Al	82	65	90	5
	Ba	104	110	102	1
	Ca	103	129	99	1
	Fe	80	106	95	1
	K	116	100	99	1
	Mg	70	85	100	0
	Mn	90	93	102	1
	Na	89	93	97	1
	Sr	101	108	100	1
ICP-MS	Ag	-	-	50.95	1
	As	93.83	108.40	88.87	4
	Cd	95.54	97.40	98.36	1
	Co	101.02	92.94	91.63	1
	Cu	99.74	102.09	94.59	1
	Ni	117.25	117.32	100.11	2
	Mo	104.90	105.49	98.68	2
	Pb	80.68	65.84	91.94	1
	Sb	104.14	113.91	96.51	1
	Zn	106.07	104.14	94.17	1
IC	Cl	-	-	116	0
	F	-	-	141	1
	NO_3	-	-	90	2
	PO_4	-	-	121	4
	SO_4	-	-	103	0

[1]Accuracy calculated from GW-HI certified reference solution
[2]Accuracy calculated from GW-LOW certified reference solution
[3]Accuracy calculated from calibration solutions

Charge Balance Error (CBE) was calculated for each sample as an additional QA/QC parameter. Nine samples exceed the -5% to 5% guideline for CBE, including CL-TP01-0.3 (-10.07%), CL-TP01-0.5 (5.16%), CL-TP01-0.6 (-12.32%), CL-TP01-0.7 (-6.56%), CL-TP01-0.9 (6.91%), CL-BHW-20-40 (-18.40%), CL-BHW-40-60 (10.43%), CL-BHW-60-80 (-6.99%). The cause of these discrepancies is not known but may be attributable to specific redox states influenced charge balance.

3.4 Mineralogy

The aqueous geochemical character of the Cart Lake tailings deposit is affected by the gangue minerals, residual primary sulfide and arsenide minerals, and their alteration products.

Thin section CL-BHE-TS-5 (0.9 m bgs, Figure 9) was identified during the investigation as having a relatively high concentration of reactive primary minerals. In particular, a visually obvious red-brown band across the middle of the thin section

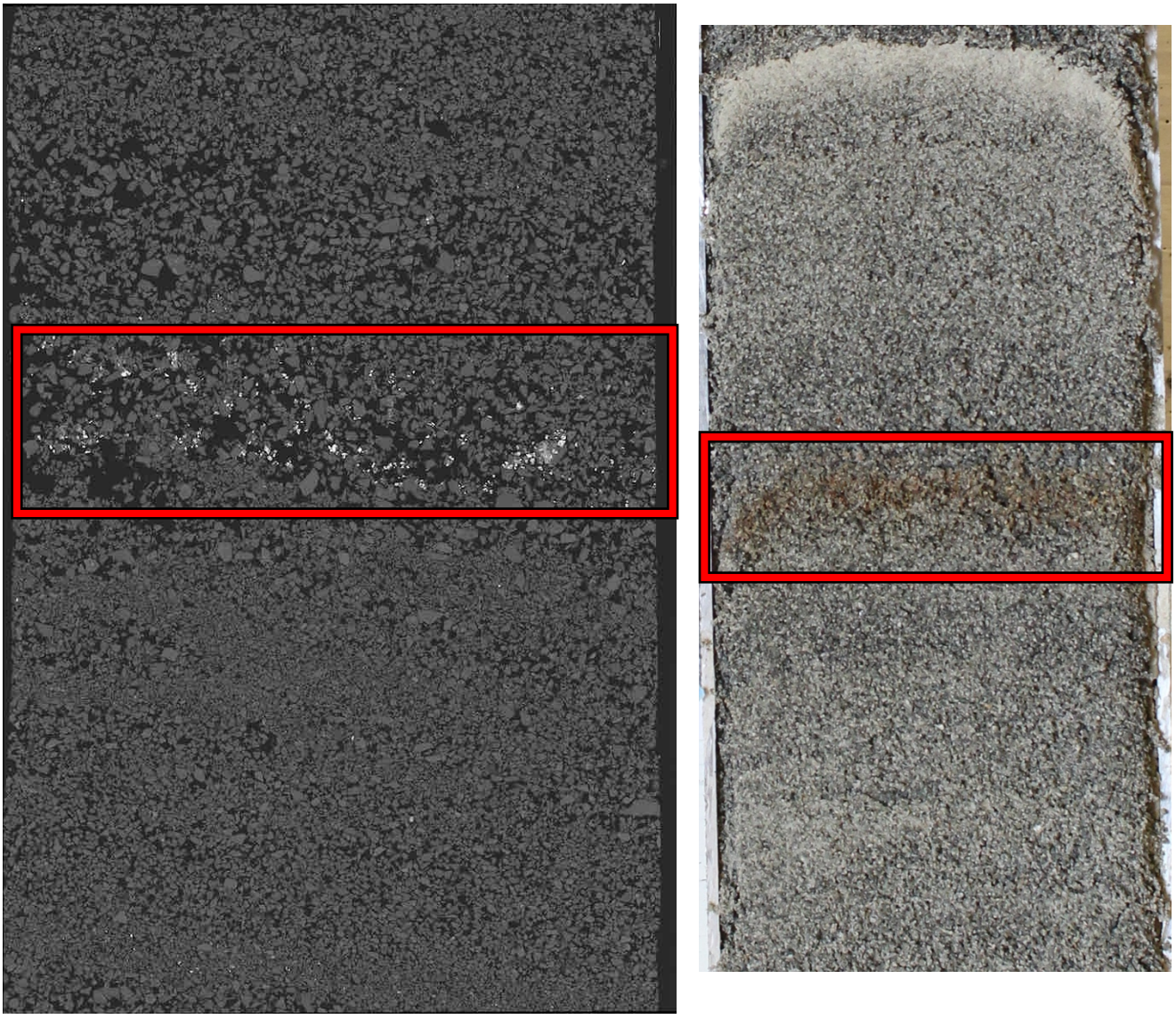

Figure 9 - Thin section TS-5 highlighting a band of high-reflectivity reactive primary minerals across the centre (Composite SEM photo and photo taken during core resin impregnation)

contains a relatively high concentration of primary minerals and associated alteration products. These red-brown minerals showed higher signal intensity in backscattered-electron SEM images (BSEI), as shown in Figure 9. The minerals in this section are representative of the mineral groups observed in the Cart Lake tailings.

3.4.1 Primary Minerals in the Cart Lake Tailings

Powder X-ray diffraction analysis of the surface crust samples collected from Cart Lake indicate the presence of primary minerals albite, calcite and chlorite, but no secondary minerals were detectable.

A total of 31 sites of interest were investigated during SEM and EMPA analysis of primary and secondary minerals from thin section CL-BHE-TS-5. Relatively unreactive primary minerals include albite, quartz, zircon, and other aluminosilicates. The principal primary reactive minerals observed and identified are calcite, pyrite, arsenopyrite, alloclasite, skutterudite solid solution members, and safflorite/löllingite/rammelsbergite solid solution members. The observed variations in composition for minerals in the safflorite(SFT)/löllingite(LLT)/rammelsbergite(RBG) solid solution series are presented in Figure 10.

Primary mineral compositions are grouped in clusters by analysis point of interest, indicative of the analysis points being collected from the same mineral grain. Atomic percentage of Ni remains low (<40%) compared to the other elements in most of these primary mineral solid solutions, with greater proportions of Fe and Co indicating most mineral grains tend towards the LLT/SFT point of the ternary diagram.

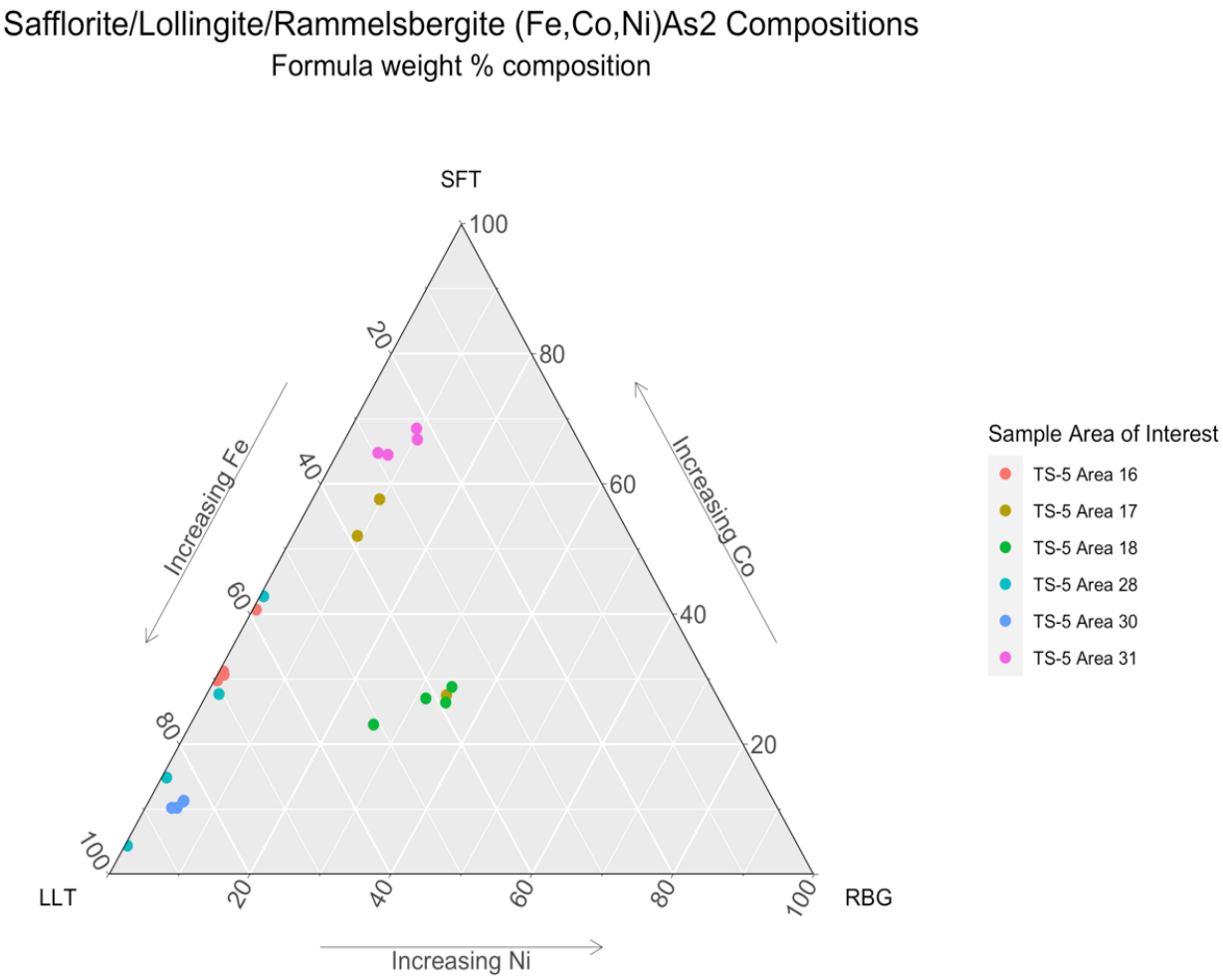

Figure 10 - Variations in observed compositions of primary reactive minerals in the safflorite/löllingite/rammelsbergite solid solution series.

3.4.2 Secondary Minerals in the Cart Lake Tailings

Secondary minerals that are observed in the Cart Lake tailings and represent primary-mineral-alteration products are classified into two compositional groups based on their dominant chemical components, including Co-As-O and Ca-Fe-As-O phases. The composition of Ca-Fe-As-O minerals is highly variable, and in this work, mineral names are only used in cases where their compositions closely matched those of known minerals.

The most ubiquitous and conclusively identified secondary mineral is a Co-As-O arsenate mineral, occurring with a grown-in-place appearance and pink to red colouring. Based on its characteristics and previous reports of the Cart Lake tailings, a high degree of certainty exists that this mineral is erythrite, a common and historically important secondary mineral that is known to occur extensively in the CMC. Examples from BSEIs are presented in Figure 11.

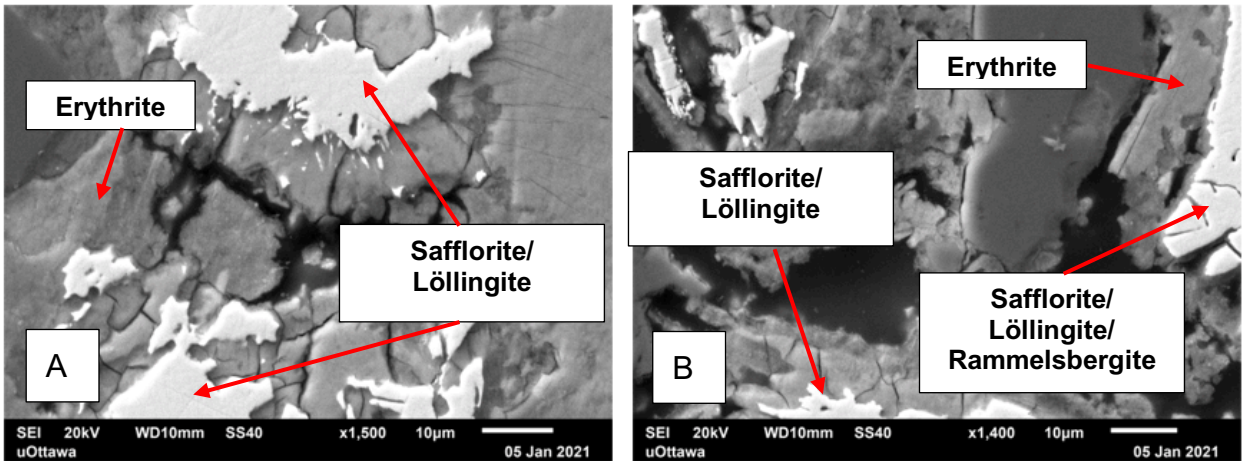

Figure 11 - SEM photos showing occurrences of erythrite adjacent to safflorite/löllingite

The Ca-Fe-As-O phases are found in weathered zones around primary sulfide and sulfarsenide grains. Several primary minerals are observed altering into these mixed-composition Ca-Fe-arsenate phases, as presented in Figure 12.

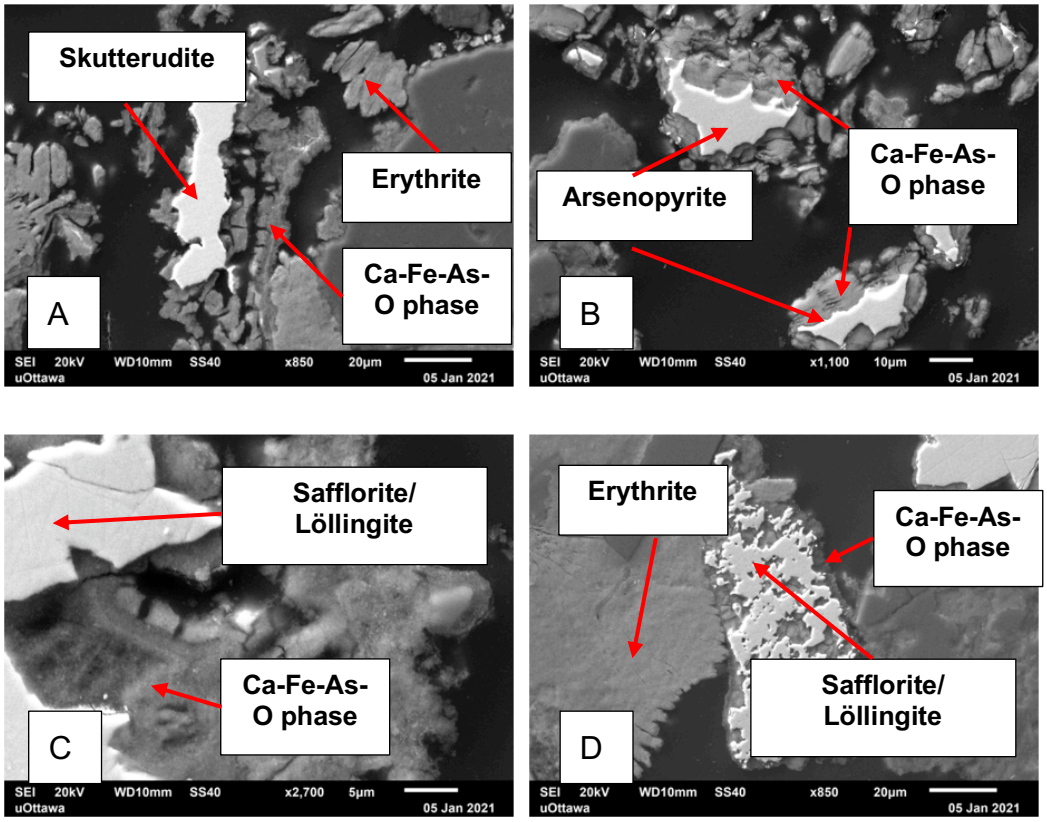

Figure 12 - BSE images showing alteration of primary minerals skutterudite (A), arsenopyrite (B), and safflorite/löllingite (C/D) into Ca-Fe-As-O phases

Ratios of Ca:Fe:As were used to further classify the minerals in this family where possible. Three possible candidates are considered for these assemblages; arseniosiderite ($Ca_2Fe_3^{3+}(AsO_4)_3O_2 \cdot 3H_2O$), yukonite ($Ca_3Fe^{3+}(AsO_4)2(OH)_3 \cdot 5H_2O$), and sewardite ($CaFe_2^{3+}(AsO_4)2(OH)_2$). Distinguishing between these three minerals is difficult, as it requires nano-scale analysis of mineral unit cells which could not be obtained with the instruments used during this project. Oxide weight % for yukonite and sewardite are not consistent in the literature, as exact compositions are difficult to establish without the use of structural methods. (Drahota et. al., 2009; King et. al., 2020; Paktunc et. al., 2015). Due to the similarity in Fe_2O_3 and CaO oxide weight % between the three candidates, differences in As_2O_5 represent the best distinguishing factor for the current project's methodology. The oxide weight % compositions of the known three Ca-Fe arsenates in comparison to the secondary mineral compositions measured by EMPA

analysis are presented in Figure 13. The three oxides displayed on the chart axes (As2O5, Fe2O3, and CaO) are the principal components.

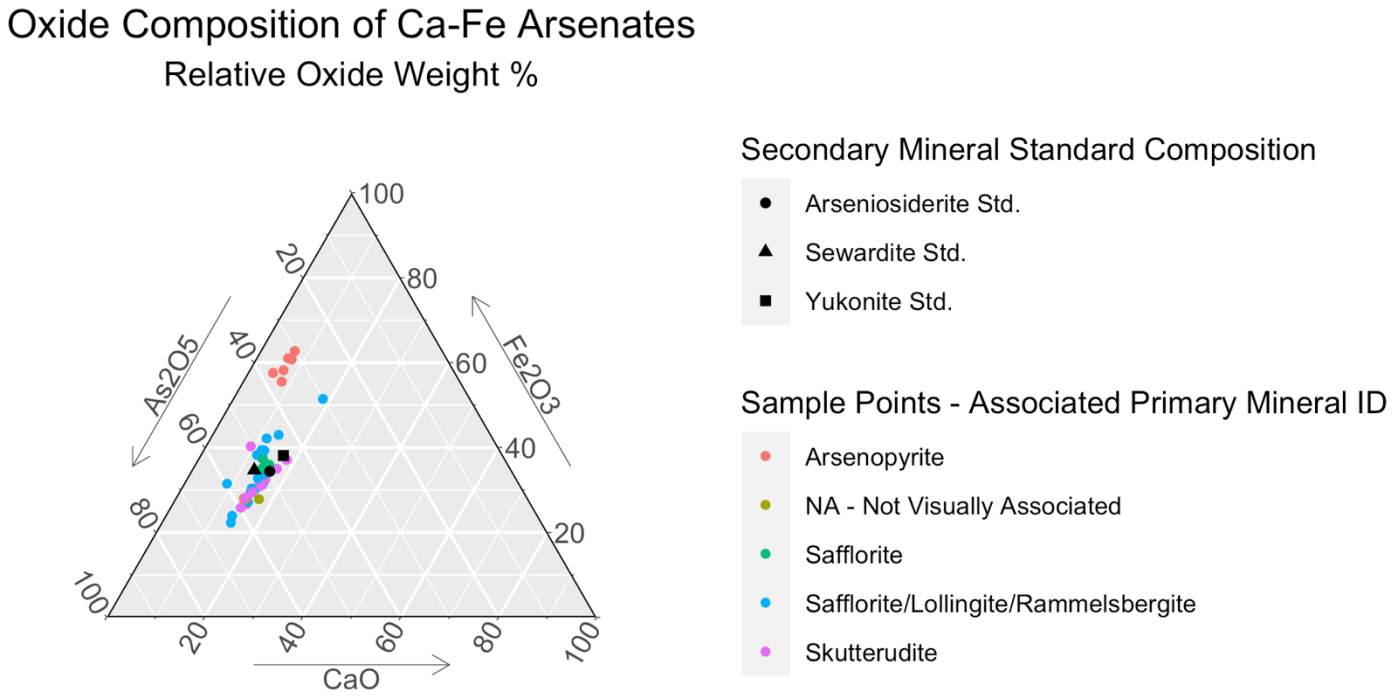

Figure 13 - Secondary mineral EMPA point analysis results relative to known Ca-Fe arsenate mineral compositions. Point colour represents the primary mineral with which the secondary mineral analysis point is associated.

The oxide weight percentages for Ca-Fe arsenates spatially associated with arsenopyrite are clustered in a group distinct from those associated with other primary minerals. The ranges of oxide weight % in Ca-Fe arsenates associated with the safflorite/löllingite/rammelsbergite and skutterudite families are generally distinct from the Ca-Fe arsenate minerals associated with arsenopyrite (20-50% Fe_2O_3, 10-20% CaO, and 30-70% As_2O_5) (Figure 13). The Ca-Fe arsenates associated with safflorite/löllingite/rammelsbergite and skutterudite are generally closer to known Ca-Fe arsenate compositions than those associated with arsenopyrite.

Relative oxide weight % compositions of As_2O_5, which show the greatest difference between the three Ca-Fe arsenate compositions, are presented in Figure 14. These

variations are presented alongside the hypothesized mineral compositions taken from webmineral.com.

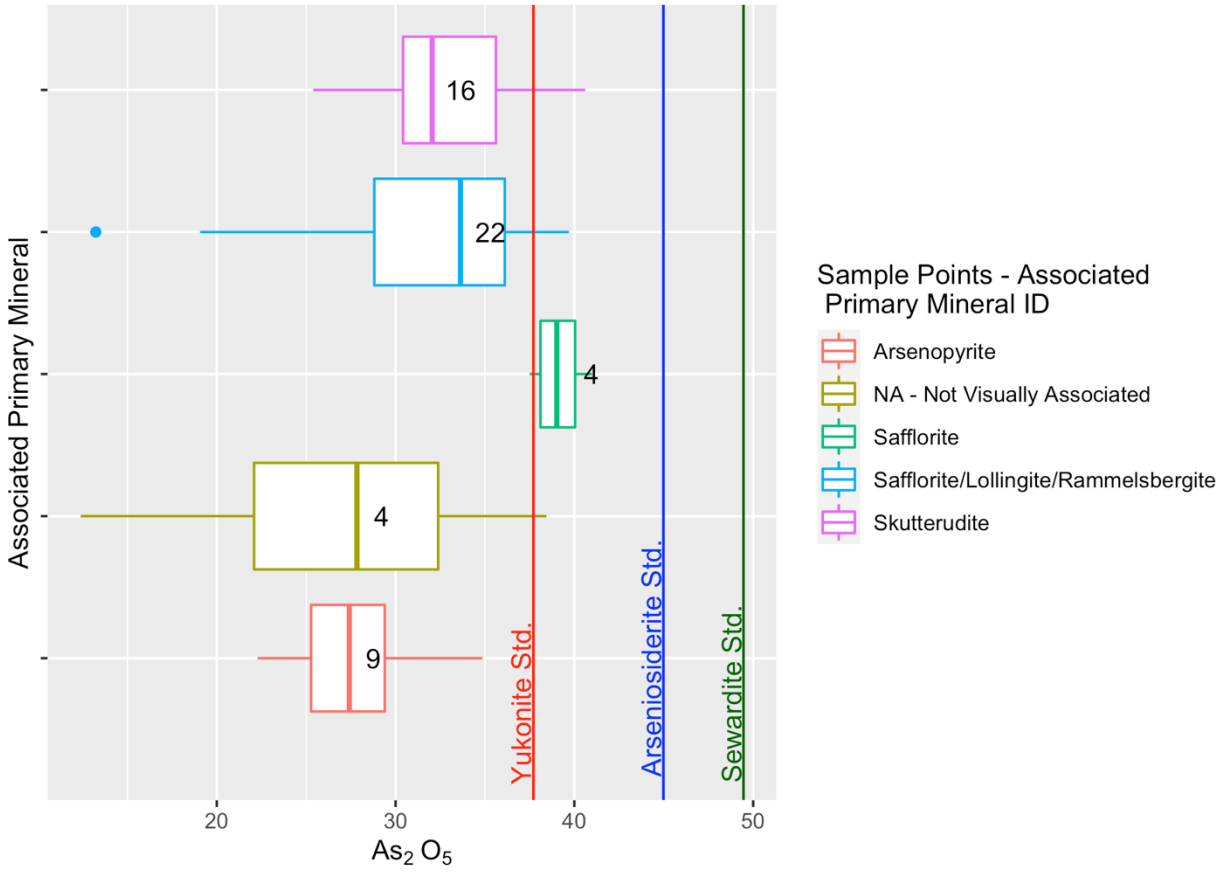

Figure 14 - Range in As2O5 oxide weight percentages collected via EMPA for secondary minerals, coloured by associated primary mineral plotted alongside expected values fro three mineral standards.. Box and whisker shapes represent the range in oxide weight % compositions, and the black numbers represent the number of analysis points

Quartile ranges in As weight % composition do not appear to align with the expected values for any of the three secondary mineral candidates. All As oxide weight percentage points associated with safflorite are within 5% of the expected composition of Yukonite, but the quartile range does not include the actual expected composition of 37.71%.

The results of EMPA point, line, and analytic map analyses are presented in Figures 13-15. Secondary mineral phases are presented in terms of their relative compositional oxide weight %, or atomic % for the analytical maps.

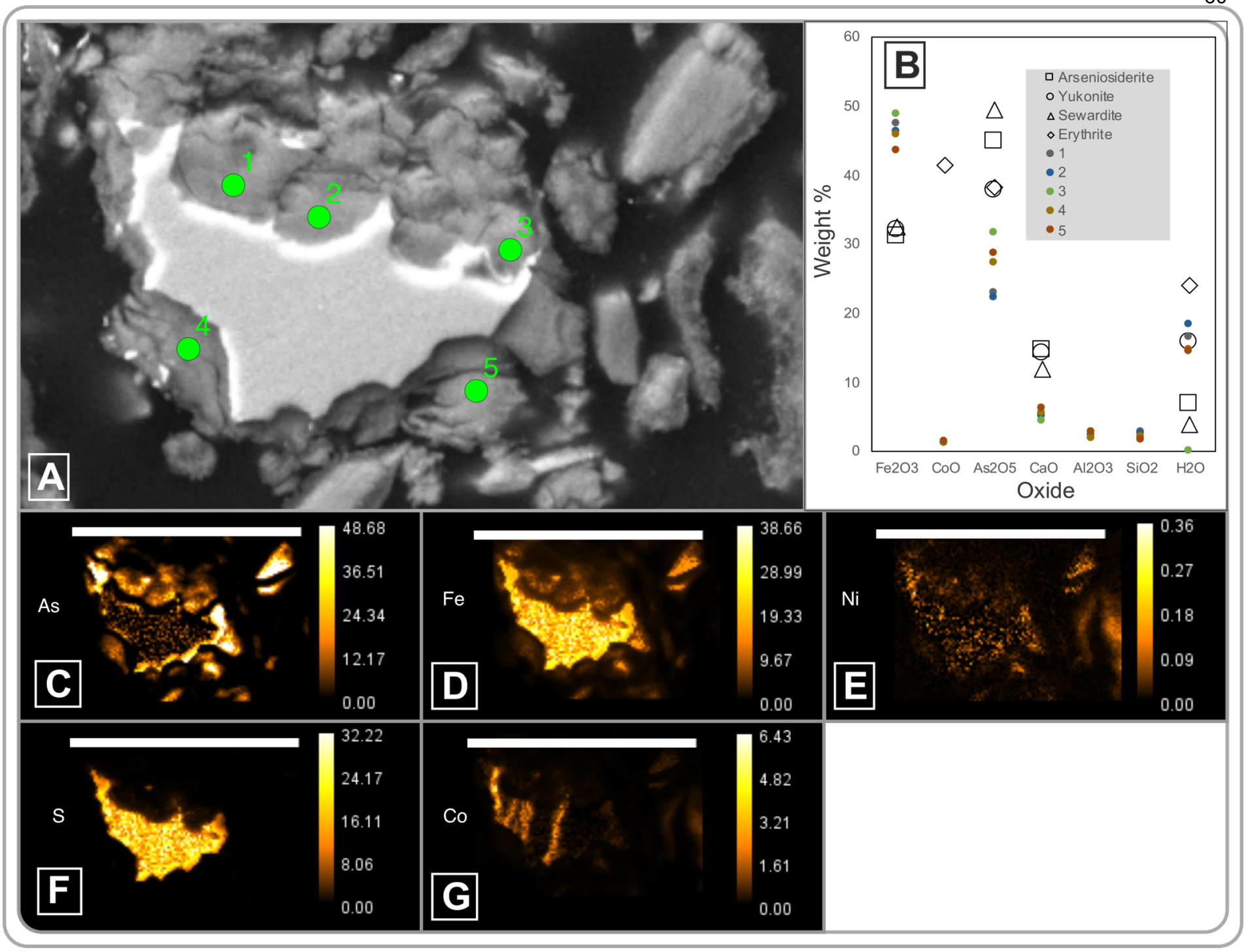

Figure 15 - EMPA analysis results - TS-5 Site of Interest 14. (A) EDS photo showing primary mineral arsenopyrite altering into mixed composition Ca-Fe arsenates. (B) EMPA point analysis results showing alteration product oxide weight % alongside expected weight % for known Ca-Fe arsenates and erythrite. (C-G) EMPA analytical maps, data shown in atomic %

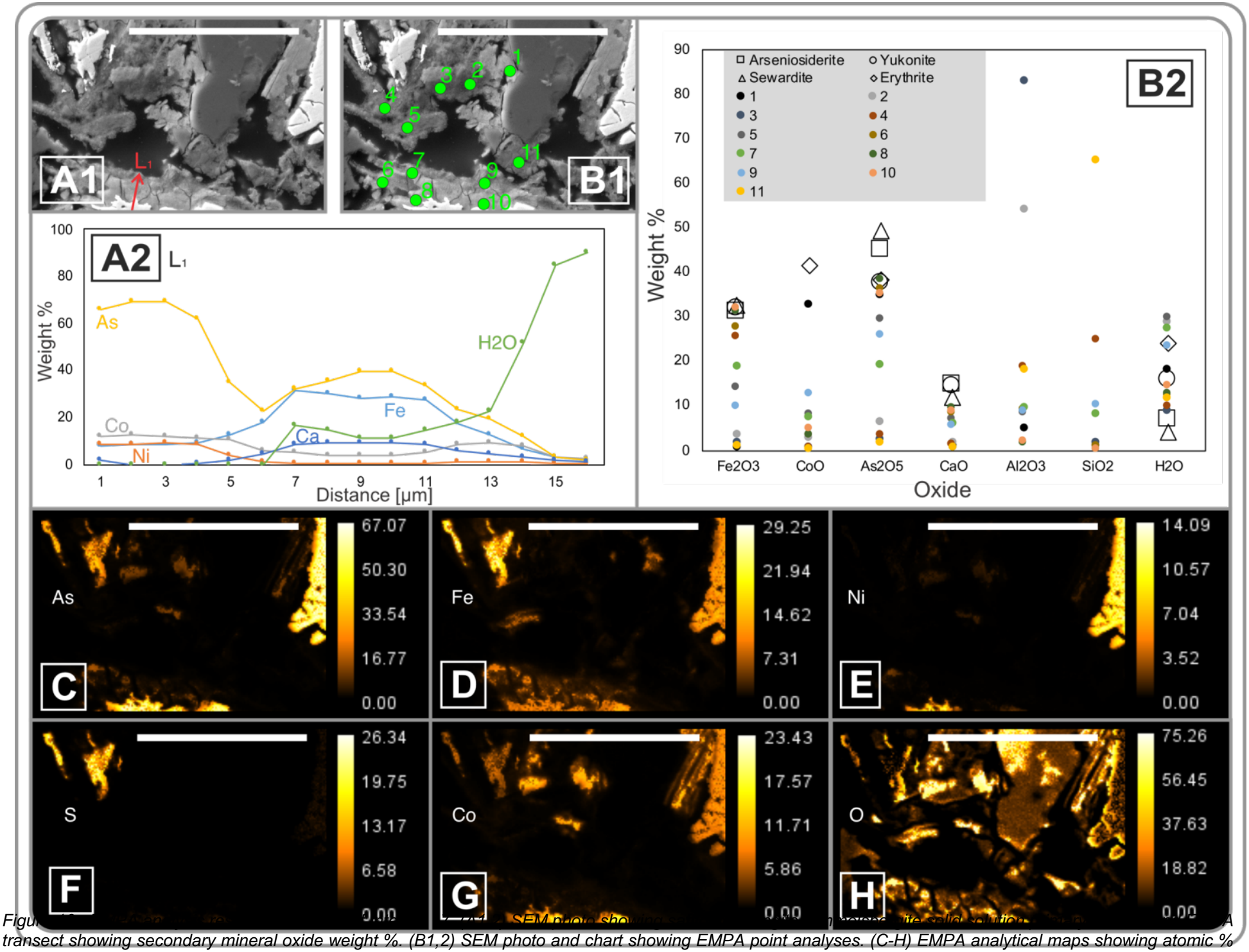

Figu[illegible] SEM photo sho[illegible] transect showing secondary mineral oxide weight %. (B1,2) SEM photo and chart showing EMPA point analyses. (C-H) EMPA analytical maps showing atomic % for As, Fe, Ni, S, Co, and O.

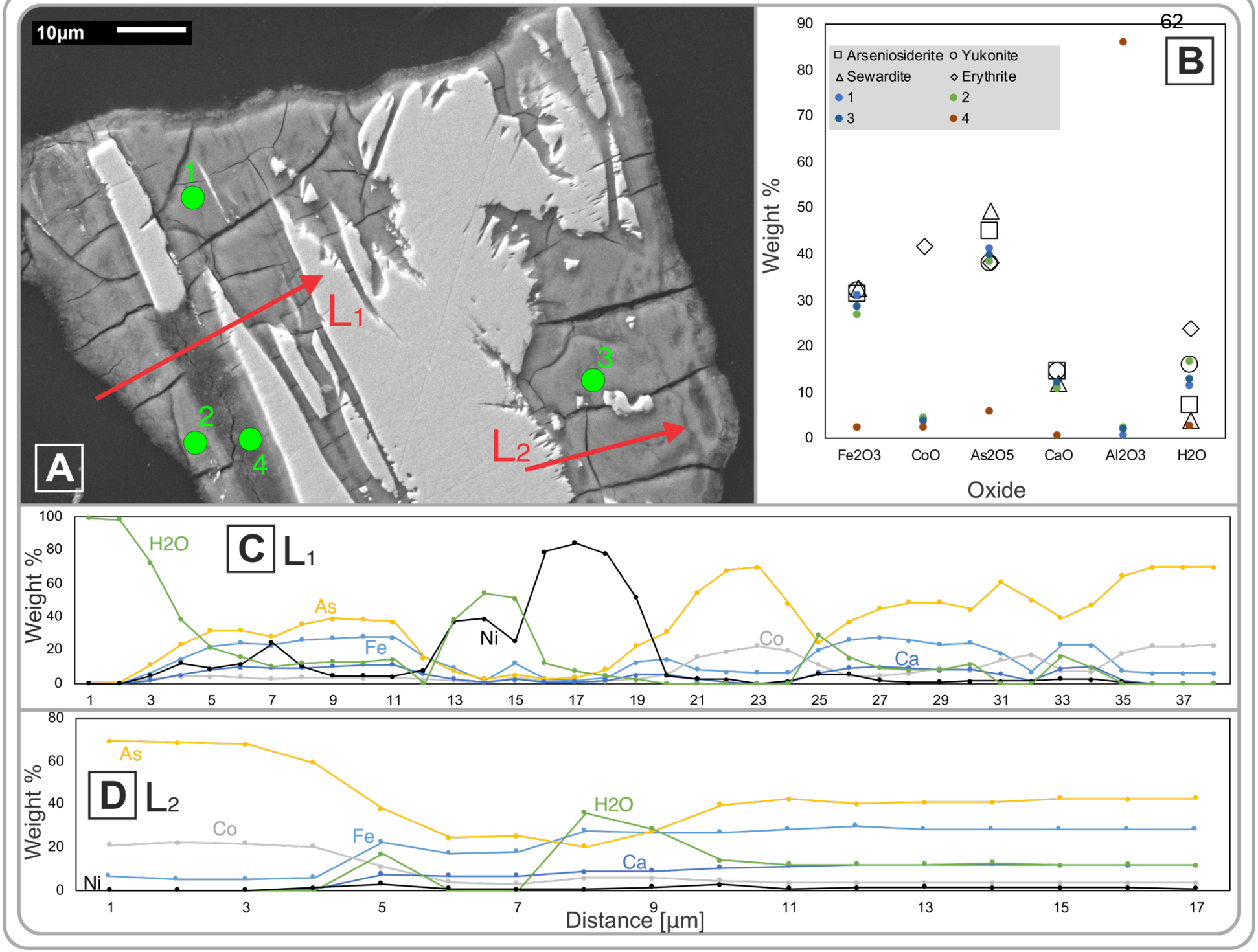

Figure 17 - EMPA analysis results - TS-5 Site of Interest 31. (A) SEM photo showing EMPA point and transect analysis locations. (B) EMPA Point analyses (C,D) EMPA transect results

Analytical maps showing atomic percentages of primary minerals indicate with a high degree of certainty the composition and identity of most primary minerals. In the case of Figure 15, approximately equal percentages of Fe, As, and S indicate approximately a 33%/33%33% division, identifying the grain as arsenopyrite. In the case of Figure 16, the variable compositions of Fe, Co, Ni, with an approximately 66% As composition identify the grain as belonging to the safflorite/löllingite/rammelsbergite solid solution.

EMPA analysis points in figures 15-17 indicate the lack of agreement between relative oxide weight compositions of Cart Lake tailings particles with the expected standard compositions from webmineral.com. Transect A2 (L1) shows As oxide weight percentages remain high (near 60%) in the primary mineral grain, then decrease by approximately half as the mineral is altered into a Ca-Fe arsenate phase. Oxide weight percentages of Ca and Fe increase in the secondary mineral, potentially indicative of absorption of these components from solution. The same trends are observed in transects C (L1) and D (L2).

3.4.3 Mineralogy QA/QC

The copper tape used to adhere the thin sections to the SEM mounting stage was used for EDS spectral calibration prior to beginning all analyses.

The identification of primary and secondary minerals was carried out using the procedures outlined in Section 2.5. Due to the limits of the analysis techniques employed, identification of these minerals with 100% accuracy was impossible. By cross-referencing the atomic % calculated by the SEM native software with the raw data analyzed using the DTSAII software package, processing errors and software issues were minimized.

The SEM EDS analyses for all elements did not include calibration with standards, and elemental data for light elements O and C are particularly subject to uncertainty from x-ray self-absorption in the sample so these elements were examined but were not used in the classification of mineral assemblages.

4 Discussion

4.1 Alteration of Primary Reactive Minerals and Characterization of Alteration Products

The reaction of As-bearing minerals, in the case of this study arsenopyrite, skutterudite, and safflorite/löllingite/rammelsbergite solid solutions with pore water yields an increase in dissolved cations in the tailings pore waters mediated by pH and Eh conditions as well as major ion balances. Biotic factors such as SO_4^{2-}, Fe, and As reducing bacteria may also exert influence over these alteration processes but were not directly studied in the current project.

No trend with depth was observed in the frequency of occurrence of secondary minerals such as erythrite or Ca-Fe arsenates, but insufficient sample size (1 core) limits conclusive identification of trends with depth or lack thereof.

Skutterudite and arsenopyrite were conclusively identified in most cases based on atomic percentage information collected during EMPA analysis. These two minerals are frequently discussed in studies of 5-element hydrothermal-origin ore veins, particularly in the mine tailings in the CMC (Clarke, 2017; Dumaresq, 2005; Kloprogge et. al., 2006; Markl et. al., 2016; Percival et. al., 2007; Petruk et. al., 1971; Scharrer et. al., 2019). Arsenopyrite, as the only primary reactive mineral containing sulfur in all studied thin sections, was identified with a high degree of confidence in all cases. Arsenide minerals with (Fe,Co,Ni):As ratios of approximately 1:2 belonging to the safflorite/löllingite/ rammelsbergite solid solution series exist within a ternary compositional gradient (Kloprogge et. al., 2006; Radcliffe and Berry, 1968). As these minerals are seldom found as pure end-members, exact compositional matches between end members and sample observations were rare. Minerals were identified as a distinct species where the fraction of a distinguishing element (Fe, Co, or Ni) was within 5% of the end-member values taken from webmineral.com (Co ≅ 21.15% for safflorite, Fe ≅ 27.15% for löllingite, and Ni ≅ 28.14% for rammelsbergite). Minerals with an (Fe,Co,Ni):As ratio of 1:3 were classified as skutterudite.

Secondary mineral families associated with the weathering of these primary minerals fall into two groups, Co-arsenate and Ca-Fe-arsenate assemblages. These two families are well documented as existing in association with primary arsenide and sulfide minerals (Bubar 2019; Drahota and Filippi, 2009; King et. al., 2020; Paktunc et. al., 2015). In the thin sections analyzed, no other distinct families are observed. Literature disagrees on exact formulas for Ca-Fe arsenates yukonite and sewardite (Pieczka et. al., 1998, Tyrrell and Graham, 1913), but they can be distinguished by analysis of crystal lattice structures (Tyrell and Graham, 1913; Jambor, 1966; Roberts et. al., 2002). This study focused on compositional analysis but the results would be complimented by discrete structural analysis with X-ray or electron-diffraction techniques.

Oxide weight percentages of secondary minerals vary to a limited degree with the associated primary mineral. The Fe content of arsenopyrite results in secondary minerals with relatively high Fe oxide weight % (50-60% Fe_2O_3, 3-10% CaO, and 30-40% As_2O_5). The Ca-Fe arsenates associated with safflorite/löllingite/rammelsbergite and skutterudite are generally closer to known Ca-Fe arsenate compositions than those associated with arsenopyrite (Figure 13). Similarity of compositions between arseniosiderite, sewardite, and yukonite limits conclusive identification of these phases.

No exact matches (within $\pm$2% of known Ca-Fe arsenate compositions) were observed in this project due to the occurrence of impurities introduced during the alteration process.

Scorodite is a commonly found alteration product associated with arsenopyrite, skutterudite, and safflorite solid solutions (Clarke, 2015; Dumaresq, 2005; Drahota et. al., 2009; Paktunc et. al., 2015; Percival et. al., 2007; Salzsauler et. al., 2005;). However, in the case of the present study no scorodite was observed surrounding any of the reactive mineral grains. This is either indicative of direct transformation from sulfarsenide minerals into Ca-Fe arsenates, or complete replacement of alteration product Fe arsenates such as scorodite by arseniosiderite as observed by Paktunc et. al., 2015.

Erythrite's grown-in-place appearance, filling gaps between tailings particles, facilitated identification and suggests Co sourcing via transport and precipitation rather than the direct result of primary mineral alteration.

4.2 Factors Influencing Dissolved Element Concentrations and Mobilization, Transport, and Attenuation Processes

4.2.1 Net Acid Generation

Acid produced through the weathering of primary reactive minerals is neutralized by buffering carbonate species sourced from the calcite-rich gangue material of these tailings. The neutralization of acidity from oxidation of residual ore minerals by carbonate minerals is well-documented and studied (Al et. al., 2000; Hiller et. al., 2013; Xu et. al., 1997).

High carbonate-mineral content in the Cart Lake tailings causes all groundwater samples to have a neutral to slightly basic pH and increases the concentration of Ca^{2+} and HCO_3^- observed in the piezometer and pore water samples.

4.2.2 Spatial distributions of dissolved elements, pH, Eh, and alkalinity

Samples collected from piezometers were used to assess the spatial distribution of pH, Eh and dissolved element concentrations across the Cart Lake tailings but no trends were observed. Deposition of tailings was likely temporally and spatially sporadic, and the multiple ore sources processed by the mills at Cart Lake results in heterogeneous distributions of the residual primary reactive minerals that influence groundwater geochemistry at Cart Lake (Dumaresq, 2005).

4.2.3 General aqueous geochemical trends

The ionic composition of the dominant cations and anions in water samples collected from the Cart Lake tailings are presented in Figure 19. The aqueous compositions indicate that Ca/HCO_3^- type waters are dominant at the surface, with an apparent shift to Ca/SO_4^{2-} type waters as depth increases. No clear difference is observed between piezometer samples and vertical pore water profile samples.

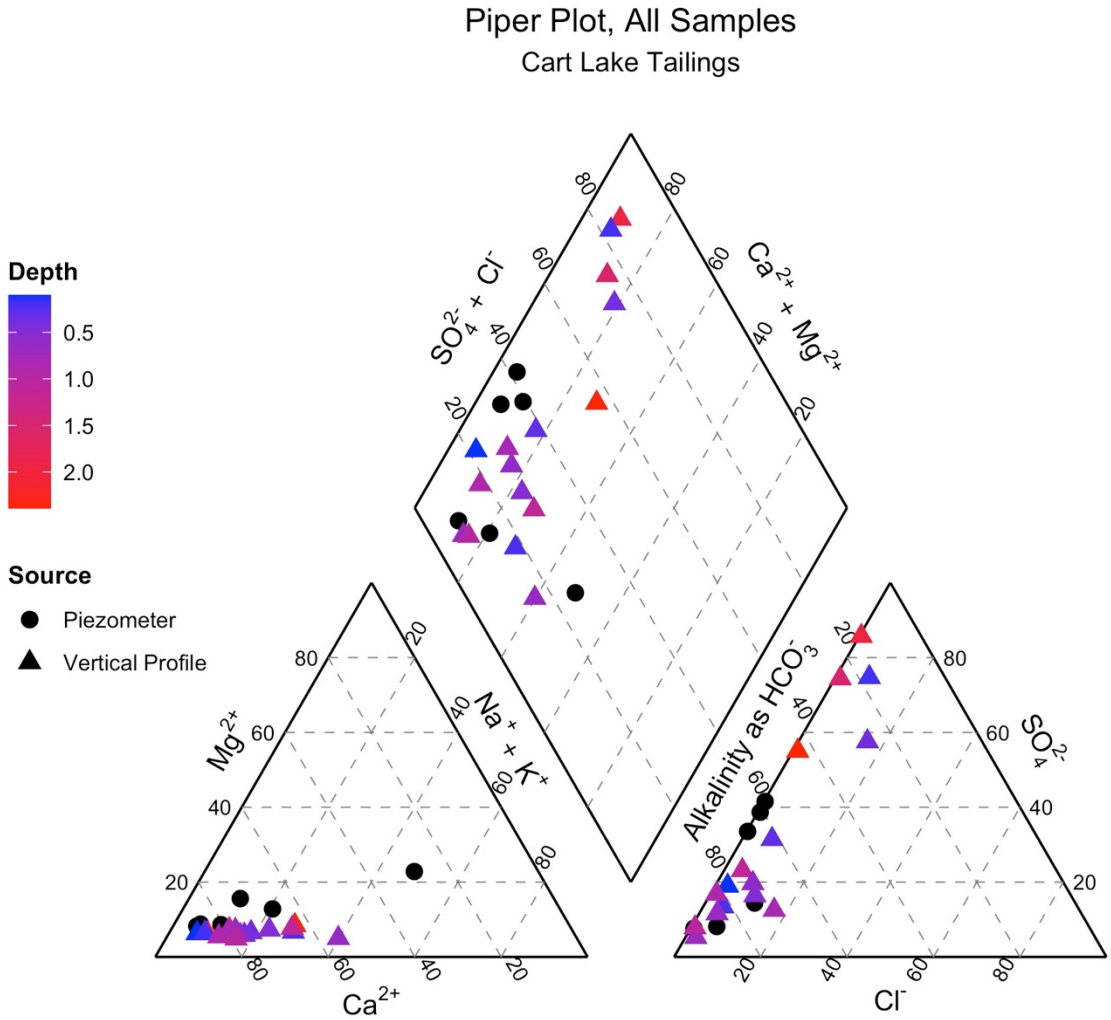

Figure 19 - Piper diagram showing major ion compositions of all samples collected from Cart Lake

4.2.4 Vertical pore water geochemical trends

Data from extracted pore water were used to analyze the vertical distributions of key geochemical parameters including pH, Eh, alkalinity, and dissolved cations and

anions. No obvious trends are observed in pH or Eh with depth, which may result from insufficient residence time for development of strong depth profiles, heterogeneous distribution of reactive minerals from spatially variable tailings deposition, or the high concentration of buffering carbonate minerals. Alkalinity values, strongly influenced by the abundant calcite gangue minerals, are highest from 0.0 to 0.7 m bgs, decrease by approximately 50% by 1.2 m bgs, and show a slow but steadily increasing trend to the deepest point in the profile. The change in alkalinity is expected to occur near the transition from the vadose to saturated zones, based on a water level measurement collection from a piezometer ~20m cross-gradient. This increase in alkalinity would be expected to proceed via reaction 5.

The degree to which SO_4^{2-} dominates major anion activity appears to be greatest at the top of the vertical profile and near the bottom, although concentrations of SO_4^{2-} and most other cations remain low in the vadose zone. The one notable exception to this trend is As, which shows a steady increase through the vadose zone and a rapid decrease just below the water table.

Increased concentrations of SO_4^{2-} and other cations just below the water table is likely attributable to a downward flow of mobilized alteration products released in the vadose zone during the summer, in which higher temperatures would be expected to increase oxidation rates. prior to sample collection. The decrease in SO_4^{2-} concentrations at the bottom of the profile may be attributable to the activity of SO_4^{2-} - reducing bacteria. Reduction of As concentrations by 50% in the vicinity of the water table is likely attributable to the precipitation of erythrite, which would be expected to remove As from solution.

At the time of sample collection, groundwater levels would be expected to be past their peak levels but not at the minimal value in the yearly cycle, suggesting the vadose zone depth would likely further increase during the year and be subject to fluctuations based on precipitation. Changes in the vadose zone depth would be expected to strongly impact these geochemical trends. Further study of the groundwater levels of Cart Lake, collected using pressure transducers installed in piezometers, would support this.

Some discrepancies were observed in the vertical geochemical profile between data collected from vertical and horizontal cores. This difference is likely attributable to the slight offset (~7m) in location between the sites of collection of both sets of cores. The heterogeneity of tailings deposition is likely sufficient to introduce differences in dissolved element concentrations between the core sections.

4.2.5 Dissolved element mobilization

Low SO_4^{2-} and dissolved cation concentrations above the water table likely results from the passivating ability of alteration rims around reactive mineral grains, as observed in previous studies (Al et al., 2000; Clarke, 2017, Nesbitt and Muir, 1998). These alteration rims would be sufficient to suppress reaction rates in the vadose zone, reducing concentrations of As, Fe, Co, SO_4^{2-}, and other dissolved elements associated with the reactive primary minerals. The almost complete surrounding of primary mineral grains by alteration products observed during EMPA analysis supports this hypothesis (Figures 10-11 & 14-16). Higher concentrations of As and Fe observed in the vadose zone compared to below the water table may be attributable to geomicrobial activity, which would increase dissolved concentrations of these elements via microbial reduction of Fe and As from alteration rims. Secondary mineral precipitation decreases concentrations of As in the saturated zone.

Elements such as Ca, Mg, Na, Co, and Ni are mobilized below the water table with As where relevant reactive primary minerals occur, but the concentrations of Co and Ni are lower (ug/L (Co, Fe, Ni) versus mg/L (As, Ca, Mg, Na)). The concentrations of these elements do not appear to be associated with changes in pH or redox potential, possibly indicating they are subject to a different controlling factor such as mineral precipitation.

Elevated concentrations of NO_3 observed near the surface of the tailings in the vertical profile may be the result of revegetation efforts on Cart Lake, during which nitrate-rich fertilizers were applied to encourage vegetation growth. Analysis of bacteriological populations in the Cart Lake tailings would confirm or refute the influence of bacteriological communities on the Cart Lake tailings.

4.2.6 Transportation

Based on general arsenic speciation trends (Lu and Zhu 2011), and the above-0 mV Eh values of the tailings pore water, the majority of dissolved As is expected to be transported as As^{5+} in the tailings pore waters. This expectation does not account for geomicrobial processes, which are well known to reduce As^{5+} in mine tailings (Amend et al. 2014, Nordstrom 2003). This would also be expected to influence Eh values, an effect not observed in the vertical profiles potentially due to obscuring geochemical processes. Geomicrobial analysis and in-field arsenic speciation analysis would support this hypothesis.

4.2.7 Attenuation

Nitrate concentrations decrease to below 10 mg/L at greater than 0.5 m bgs. This decrease in NO_3^- is likely attributable to reduction by NO_3^--reducing bacteria, a well-studied and understood phenomenon in mine tailings (Burt et. al., 1999; Rivett et. al., 2008; Thayalakumaran et al., 2008).

Erythrite precipitation and primary mineral alteration into Ca-Fe arsenates, moderated by Eh and pH conditions, is likely one of the primary processes controlling As concentrations in solution and may be responsible for decreasing As concentrations by more than 50% below the water table. A simplified reaction showing precipitation of erythrite is presented in Reaction 7. Coprecipitation and adsorption of As onto Fe-oxyhydroxides is a well-known As-attenuating process in mine tailings and is suspected to occur in the Cart Lake tailings, but no clear examples of this were identified in project samples despite the well-documented occurrence of these reactions in mine tailings (Blowes and Jambor 1990; Clarke, 2017; Dumaresq, 2005; Sprague and Vermaire, 2018). As attenuation by adsorption to Fe-oxyhydroxides, if occurring, would be limited by low dissolved Fe oxyhydroxide content in these tailings.

Incorporation of Ca into alteration rims surrounding primary reactive mineral grains results in the formation of Ca-Fe arsenate minerals, removing Ca from solution. Future geochemical modelling would suggest equilibrium concentrations of Ca with respect to Ca-Fe arsenates and gangue minerals such as calcite.

All primary minerals observed in this study, containing Fe or not, were observed to be in close contact with or surrounded by Ca-Fe arsenates. The Fe contained in Ca-Fe arsenate mineral assemblages sources directly from Fe-containing primary mineral grains where such grains are present (pyrite and arsenopyrite), and to a lesser extent from solution in the absence of Fe in the primary mineral. Arsenate mineral formation is expected to also remove aqueous Fe(III) from solution via incorporation into Ca-Fe arsenates throughout the saturated portion of the water column. Concentrations of Fe may be a limiting factor during erythrite precipitation in the presence of excess Co. Rates of sulfide and arsenide mineral alteration into Ca-Fe arsenates may also be limited by low Fe concentrations in the tailings pore waters. A previous study observed that these alteration rates are likely also kinetically controlled (Paktunc et. al., 2015).

Since one mole of Co is released by dissolution of safflorite, and three moles of Co are required for the precipitation of one mole of erythrite, direct alteration of safflorite (and other arsenide minerals containing only one or two Co formula units) into erythrite is unlikely, supporting Co sourcing via incorporation from solution rather than direct alteration. Dissolution of safflorite and precipitation of erythrite would be expected to proceed via reaction 6 and 7 (Markl et. al., 2014).

$$(6) \quad CoAs_{2(safflorite)} + 2H_2O + 3O_2 \rightarrow Co^{2+} + 2H_2AsO_4^-$$

$$(7) \quad 3Co^{2+} + 2H_2AsO_4^- + 8H_2O \rightarrow Co_3(AsO_4)_2 \bullet 8(H_2O)_{(erythrite)} + 4H^+$$

The persistence and fate of dissolved elements in the Cart Lake tailings are subject to a variety of factors, including geomicrobial and geochemical influences. Further studies might investigate the specific roles of geomicrobial populations, cation speciation, and reaction kinetics to complete the understanding of the processes controlling dissolved elements in the Cart Lake tailings.

5 Conclusions

Uncontained residual mine tailings deposited in Cart Lake contribute elevated concentrations of As to groundwater via oxidative dissolution of reactive primary sulfide and sulfarsenide minerals. This study aims to determine the factors controlling mobilization, transportation, and attenuation of As in the Cart Lake tailings via groundwater characterization, mineralogical analysis, and interpretation of the intersection between the two.

Water samples collected from previously existing piezometers and from pore water extracted from tailings cores were analyzed via ICP-MS, ICP-OES, and IC to measure dissolved cation and anion concentrations. Mineralogical investigations were carried out using a combination of binocular microscopy, SEM-EDS analyses, and EMPA analyses. The groundwater in Cart Lake shows evidence of sulfide-affected tailings subject to carbonate buffering, with pH ranging from 6.7 to 8.6, Eh ranging from 46 to 210 mV, and alkalinity ranging from 32 to 201 mg/L HCO_3^-. The dominant cation species are Ca (4.9 to 192.0 mg/L), K (1.1 to 13.5 mg/L), Mg (1.2 to 8.7 mg/L), and Na (2.1 to 16.9 mg/L) and the dominant anionic species are alkalinity, As (0.003 to 18.1 mg/L), Cl^- (0.3 to 16.8 mg/L), PO_4 (0.04. to 9.6 mg/L), and SO_4^{2-} (6.8 to 456.1 mg/L). Concentrations of minor and trace cations such as Fe, Co, and Ni are present at the μg/L scale. The prevalent primary reactive minerals observed in the tailings are arsenopyrite, pyrite, skutterudite, and safflorite/löllingite/rammelsbergite solid solutions. Alteration products of these minerals include Ca-Fe arsenates and Co-arsenates such as arseniosiderite and erythrite respectively.

The acid-generating potential of these tailings, resulting from the oxidative dissolution of arsenopyrite and pyrite, is neutralized by alkalinity species supplied in abundance by gangue minerals, principally HCO_3^-. Precipitation and primary mineral alteration reactions remove As, Fe, and Ca from pore water, resulting in the formation of Ca-Fe arsenates and Co-As arsenates. Compositions of secondary minerals in the Ca-Fe arsenate family were compared to those of known Ca-Fe arsenate mineral phases arseniosiderite, sewardite, and yukonite based on EMPA data. Spatial relationships

between primary mineral types and secondary mineral compositions were also investigated, suggesting Fe-Ca arsenates associated with arsenopyrite generally showed greater relative Fe oxide weight % than the other primary minerals. Further classification into distinct Ca-Fe arsenate phases would require structural investigation.

Reactive primary mineral grains found in the Cart Lake tailings may be passivated by surrounding alteration rims above the water table, reducing concentrations of SO_4^{2-} in the vadose zone. Concentrations of As and Fe reach their highest values above the water table subject to geomicrobial influences. Just below the water table, the passivating ability of these reaction rims would be reduced. This, as well as transportation of mobilized elements from the vadose zone, leads to increased concentrations of many minor and trace cations and anions associated with reactive primary minerals just below the water table.

Geochemical modelling would indicate the extent to which secondary minerals reduce concentrations of major, minor, and trace cations as pore water travels through the vertical profile. In-field analysis of SO_4^{2-}, Fe(III)/Fe(II), and As(III)/As^{5+} would provide further information regarding the redox chemistry of water samples, required for accurate geochemical modeling. Structural analysis of Ca-Fe arsenates would enable further classification into distinct families. Analysis of biological communities in the Cart Lake tailings would further inform conclusions regarding As and Fe redox states, and the eventual fate of dissolved contaminants.

References

Al, Tom A., Chris J. Martin, and David W. Blowes. 2000. “Carbonate-Mineral/Water Interactions in Sulfide-Rich Mine Tailings.” Geochimica et Cosmochimica Acta 64 (23): 3933–48. https://doi.org/10.1016/S0016-7037(00)00483-X.

Amend, Jan P., Chad Saltikov, Guang Sin Lu, and Jaime Hernandez. 2014. “Microbial Arsenic Metabolism and Reaction Energetics.” Reviews in Mineralogy and Geochemistry 79 (1): 391–433. https://doi.org/10.2138/rmg.2014.79.7.

Anderson, Pat. 1993. “Cobalt Mining Camp Tailings Inventory Cobalt, Ontario.”

Andrade, C. F., Heather E. Jamieson, T. K. Kyser, Tanmay Praharaj, and Danielle Fortin. 2010. “Biogeochemical Redox Cycling of Arsenic in Mine-Impacted Lake Sediments and Co-Existing Pore Waters near Giant Mine, Yellowknife Bay, Canada.” Applied Geochemistry 25 (2): 199–211. https://doi.org/10.1016/j.apgeochem.2009.11.005.

Andrews, A. J., L. Owsiacki, R. Kerrich, and D. F. Strong. 1986. “The Silver Deposits at Cobalt and Gowganda, Ontario. I: Geology, Petrography, and Whole-Rock Geochemistry.” Canadian Journal of Earth Sciences. https://doi.org/10.1139/e86-143.

Baker, Brett J., and Jillian F. Banfield. 2003. “Microbial Communities in Acid Mine Drainage.” FEMS Microbiology Ecology 44 (2): 139–52. https://doi.org/10.1016/S0168-6496(03)00028-X.

Beauchemin, S., and John Y. T. Kwong. 2006. “Impact of Redox Conditions on Arsenic Mobilization from Tailings in a Wetland with Neutral Drainage.” Environmental Science and Technology 40 (20): 6297–6303. https://doi.org/10.1021/es0609001.

Bowell, Robert J., Charles N. Alpers, Heather E. Jamieson, D. Kirk Nordstrom, and Juraj Majzlan. 2014. “The Environmental Geochemistry of Arsenic - An Overview.” Reviews in Mineralogy and Geochemistry 79 (1): 1–16. https://doi.org/10.2138/rmg.2014.79.1.

Bowell, Robert J., N. H. Morley, and V. K. Din. 1994. “Arsenic Speciation in Soil Porewaters from the Ashanti Mine, Ghana.” Applied Geochemistry 9 (1): 15–22. https://doi.org/10.1016/0883-2927(94)90048-5.

Boyle, R. W., and A. S. Dass. 1971. “The Origin of the Native Silver Veins at Cobalt, Ontario.” The Canadian Mineralogist 11 (1): 414–29. http://canmin.geoscienceworld.org/content/11/1/414.short.

Buckley, Alan N., and Grayson W. Walker. 1988. “The Surface Composition of Arsenopyrite Exposed to Oxidizing Environments.” Applied Surface Science 35 (2): 227–40. https://doi.org/10.1016/0169-4332(88)90052-9.

Campbell, Kate, and Darrell Nordstrom. 2014. “Arsenic Speciation and Sorption in Natural Environments.” Reviews in Mineralogy and Geochemistry 79 (October): 185–216. https://doi.org/10.2138/rmg.2014.79.3.

Card, K. D., W. H. McIwaine, and H. D. Meyn. 1973. “Geology of the Maple Mountain Area, Districts of Timiskaming, Nipissing, and Sudbury.” Ministry of Natural Resources 106: 1–800.

Casiot, Corinne, Guillaume Morin, Farid Juillot, Odile Bruneel, Jean Christian Personné, Marc Leblanc, Katia Duquesne, Violaine Bonnefoy, and Françoise Elbaz-Poulichet. 2003. “Bacterial Immobilization and Oxidation of Arsenic in Acid Mine Drainage (Carnoulès Creek, France).” Water Research 37 (12): 2929–36. https://doi.org/10.1016/S0043-1354(03)00080-0.

Clarke, Jeff. 2017. “THE CHARACTERIZATION OF ARSENIC MINERAL PHASES FROM LEGACY MINE WASTE AND SOIL NEAR COBALT, ONTARIO.”

Cooper, Stancil. 1941. “The Mixed Indicator Bromocresol Green-Methyl Red for Carbonates in Water.” Industrial and Engineering Chemistry - Analytical Edition 13 (7): 466–70. https://doi.org/10.1021/i560095a011.

Craw, Dave, and Robert J. Bowell. 2014. “The Characterization of Arsenic in Mine Waste.” Reviews in Mineralogy and Geochemistry 79 (1): 473–505. https://doi.org/10.2138/rmg.2014.79.10.

Dumaresq, Charles G. 2005. “The Occurrence of Arsenic and Heavy Metal Contamination from Natural and Anthropogenic Sources in the Cobalt Area of Ontario,” no. November: 309.

Filippi, Michal, Petr Drahota, Vladimír Machovič, Vlasta Böhmová, and Martin Mihaljevič. 2015. “Arsenic Mineralogy and Mobility in the Arsenic-Rich Historical Mine Waste Dump.” Science of the Total Environment 536: 713–28. https://doi.org/10.1016/j.scitotenv.2015.07.113.

Hiller, Edgar, Marián Petrák, Roman Tóth, Bronislava Lalinská-Voleková, Ľubomír Jurkovič, Gabriela Kučerová, Anežka Radková, Peter Šottník, and Jaroslav Vozár. 2013. “Geochemical and Mineralogical Characterization of a Neutral, Low-Sulfide/High-Carbonate Tailings Impoundment, Markušovce, Eastern Slovakia.” Environmental Science and Pollution Research 20 (11): 7627–42. https://doi.org/10.1007/s11356-013-1581-5.

Jambor, J.L. (1966) Re-examination of yukonite. The Canadian Mineralogist: 8: 667.

Jambor, J. L. 1971a. “Distribution of Some Minor Elements in the Nipissing Diabase.” The Canadian Mineralogist 11 (1): 320–57. https://doi.org/10.1088/1751-8113/44/8/085201.

Jambor, J. L. 1971b. “Origin of the Silver Veins of the Cobalt-Gowganda Region.” The Canadian Mineralogist 11 (1918): 402–13.

Jambor, J. L. 1971c. “The Nipissing Diabase.” The Canadian Mineralogist 11 (1): 34–75.

Kelly, J., P. Champagne, and Frederick A. Michel. 2007. “Assessment of Metal Attenuation in a Natural Wetland System Impacted by Alkaline Mine Tailings , Cobalt , Ontario , Canada.” Mine Water and the Environment 26: 181–90. https://doi.org/10.1007/s10230-007-0007-3.

King, Graham, Mert Celikin, Mario Alberto Gomez, Levente Becze, Valeri Petkov, and Giancarlo Della Ventura. 2020. “Revealing the Structures and Relationships of Ca(Ii)-Fe(Iii)-AsO4minerals: Arseniosiderite and Yukonite.” *Environmental Science: Nano* 7 (12): 3735–45. https://doi.org/10.1039/d0en00503g.

Kloprogge, J. T., L. V. Duong, M. Weier, and W. N. Martens. 2006. “Nondestructive Identification of Arsenic and Cobalt Minerals from Cobalt City, Ontario, Canada: Arsenolite, Erythrite, and Spherocobaltite on Pararammelsbergite.” Applied Spectroscopy 60 (11): 1293–96. https://doi.org/10.1366/000370206778999148.

Kissin, S. A. 1992. “Five-Element (Ni-Co-As-Ag-Bi) Veins.” Geoscience Canada.

Kramer, James R., Nicholas W.H. Adams, Helen Manolopoulos, and Pamela V. Collins. 1999. “Silver at an Old Mining Camp, Cobalt, Ontario, Canada.” Environmental Toxicology and Chemistry 18 (1): 23–29. https://doi.org/10.1897/1551-5028(1999)018<0023:SAAOMC>2.3.CO;2.

Kwong, John Y. T., S. Beauchemin, M. F. Hossain, and W. D. Gould. 2007. “Transformation and Mobilization of Arsenic in the Historic Cobalt Mining Camp, Ontario, Canada.” Journal of Geochemical Exploration 92 (2–3): 133–50. https://doi.org/10.1016/j.gexplo.2006.08.002.

Legun, Andrew. 1984. “Huronian Stratigraphy and Sedimentation in the Cobalt Area.” Ontario Geological Survey. Vol. 5508. https://doi.org/10.1021/nl904053j.

Lengke, Maggy F., Charoen Sanpawanitchakit, and Regina N. Tempel. 2009. “The Oxidation and Dissolution of Arsenic-Bearing Sulfides.” Canadian Mineralogist 47 (3): 593–613. https://doi.org/10.3749/canmin.47.3.593.

Lu, Peng, and Chen Zhu. 2011. “Arsenic Eh-PH Diagrams at 25°C and 1 Bar.” Environmental Earth Sciences 62 (8): 1673–83. https://doi.org/10.1007/s12665-010-0652-x.

Marin, A. R., P. H. Masscheleyn, and W. H. Patrick. 1993. “Soil Redox-PH Stability of Arsenic Species and Its Influence on Arsenic Uptake by Rice.” Plant and Soil 152 (2): 245–53. https://doi.org/10.1007/BF00029094.

Markl, Gregor, Mathias Burisch, and Udo Neumann. 2016. “Natural Fracking and the Genesis of Five-Element Veins.” Mineralium Deposita 51 (6): 703–12. https://doi.org/10.1007/s00126-016-0662-z.

Markl, Gregor, Michael A.W. Marks, Insa Derrey, and Jan Erik Gühring. 2014. “Weathering of Cobalt Arsenides: Natural Assemblages and Calculated Stability Relations among Secondary Ca-Mg-Co Arsenates and Carbonates.” American Mineralogist 99 (1): 44–56. https://doi.org/10.2138/am.2014.4540.

Masscheleyn, Patrick H., Ronald D. Delaune, and William H. Patrick. 1991. “Effect of Redox Potential and PH on Arsenic Speciation and Solubility in a Contaminated Soil.” Environmental Science and Technology 25 (8): 1414–19. https://doi.org/10.1021/es00020a008.

Michel, Frederick A., and Kringen Henein. 2007. “Natural Re-Vegetation of Arsenic-Bearing Alkaline Tailings At Cobalt , Ontario 1.”

Moses, Carl O., D. Kirk Nordstrom, Janet S. Herman, and Aaron L. Mills. 1987. “Aqueous Pyrite Oxidation by Dissolved Oxygen and by Ferric Iron.” Geochimica et Cosmochimica Acta 51 (6): 1561–71. https://doi.org/10.1016/0016-7037(87)90337-1.

Nesbitt, H. W. 1998. “Oxidation States and Speciation of Secondary Products on Pyrite and Arsenopyrite Reacted with Mine Waste Waters and Air.” Mineralogy and Petrology 62 (1–2): 123–44. https://doi.org/10.1007/BF01173766.

Nordstrom, D. Kirk, Juraj Majzlan, and Erich Königsberger. 2014. “Thermodynamic Properties for Arsenic Minerals and Aqueous Species.” Reviews in Mineralogy and Geochemistry 79 (1): 217–55. https://doi.org/10.2138/rmg.2014.79.4.

Nordstrom, D.K. 2003. “Effects of Microbiological and Geochemical Interactions in Mine Drainage, Environmental Aspects of Mine Wastes.” Mineralogical Association of Canada 31 (January): 227–38.

Paktunc, Dogan, Juraj Majzlan, Artis Huang, Yves Thibault, Michel B. Johnson, and Mary Anne White. 2015. “Synthesis, Characterization, and Thermodynamics of Arsenates Forming in the Ca-Fe(III)-As(V) -NO3 System: Implications for the Stability of Ca-Fe Arsenates.” American Mineralogist 100 (8–9): 1803–20. https://doi.org/10.2138/am-2015-5199.

Paikaray, Susanta. 2015. “Arsenic Geochemistry of Acid Mine Drainage.” Mine Water and the Environment 34 (2): 181–96. https://doi.org/10.1007/s10230-014-0286-4.

Percival, Jeanne B., John Y. T. Kwong, Charles G. Dumaresq, and Frederick A. Michel. 2007. “DISTRIBUTION OF AS, NI AND CO IN TAILINGS AND SURFACE WATERS IN THE COBALT AREA, ONTARIO.”

Petruk, William. 1971a. “Depositional History of the Ore Minerals.” The Canadian Mineralogist 11 (1): 396–401.

———. 1971b. “Mineralogical Characteristics of the Deposits and Textures of the Ore Minerals.” The Canadian Mineralogist 11 (1): 108–39.

Petruk, William, J. L. Jambor, and R. W. Boyle. 1971. “History of the Cobalt and Gowganda Area.” The Canadian Mineralogist 11 (1): 1–11. https://pubs.geoscienceworld.org/canmin/article/11/1/1/10814/history-of-the-cobalt-and-gowganda-area.

Petrunic, Barbara M., Tom A. Al, and Louise Weaver. 2006. “A Transmission Electron Microscopy Analysis of Secondary Minerals Formed in Tungsten-Mine Tailings with an Emphasis on Arsenopyrite Oxidation.” Applied Geochemistry 21 (8): 1259–73. https://doi.org/10.1016/j.apgeochem.2006.06.003.

Praharaj, Tanmay, and Danielle Fortin. 2004. “Indicators of Microbial Sulfate Reduction in Acidic Sulfide-Rich Mine Tailings.” Geomicrobiology Journal 21 (7): 457–67. https://doi.org/10.1080/01490450490505428.

———. 2008. “Seasonal Variations of Microbial Sulfate and Iron Reduction in Alkaline Pb-Zn Mine Tailings (Ontario, Canada).” Applied Geochemistry 23 (12): 3728–40. https://doi.org/10.1016/j.apgeochem.2008.09.008.

Radcliffe, D., and L. G. Berry. 1968. “The Safflorite-Loellingite Solid Solution Series.” American Mineralogist 53 (11–12): 1856–81.

Ried, D. Fraser, J. J. Denny, and R. H. Hutchison. 1923. “Milling and Metallurgical Practice in Treatment of Silver Ores at Cobalt.” Toronto.

Rivett, Michael O., Stephen R. Buss, Philip Morgan, Jonathan W.N. Smith, and Chrystina D. Bemment. 2008. “Nitrate Attenuation in Groundwater: A Review of Biogeochemical Controlling Processes.” Water Research 42 (16): 4215–32. https://doi.org/10.1016/j.watres.2008.07.020.

Ruzicka, V., and R.I. Thorpe. 2015. “Arsenide Vein Silver, Uranium.” Geology of Canadian Mineral Deposit Types 8: 287–306. https://doi.org/10.1130/dnag-gna-p1.287.

Roberts, A.C., Cooper, M.A., Hawthorne, F.C., Criddle, A.J., Stirling, J.A.R. (2002) Sewardite, CaFe3+2(AsO4)2(OH)2, the Ca-analogue of carminite, from Tsumeb, Namibia: description and crystal structure. Canadian Mineralogist: 40: 1191-1198.

Salzsauler, Kristin A., Nikolay V. Sidenko, and Barbara L. Sherriff. 2005. “Arsenic Mobility in Alteration Products of Sulfide-Rich, Arsenopyrite-Bearing Mine Wastes, Snow Lake, Manitoba, Canada.” Applied Geochemistry 20 (12): 2303–14. https://doi.org/10.1016/j.apgeochem.2005.06.007.

Scharrer, Manuel, Stefan Kreissl, and Gregor Markl. 2019. “The Mineralogical Variability of Hydrothermal Native Element-Arsenide (Five-Element) Associations and the Role of Physicochemical and Kinetic Factors Concerning Sulfur and Arsenic.” Ore Geology Reviews 113 (June): 103025. https://doi.org/10.1016/j.oregeorev.2019.103025.

Schenk, P. E. 1965. “Depositional Environment of the Gowganda Formation (Precambrian) at the South End of Lake Tamigami, Ontario.” Journal of Sedimentary Research 35 (2): 309–18. https://doi.org/10.1306/74d7125d-2b21-11d7-8648000102c1865d.

Smyk, M. C., and D. H. Watkinson. 1990. “Sulfide Remobilization in Archean Volcano-Sedimentary Rocks and Its Significance in Proterozoic Silver Vein Genesis, Cobalt, Ontario.” Canadian Journal of Earth Sciences 27 (9): 1170–81. https://doi.org/10.1139/e90-124.

Sprague, Dale D., Frederick A. Michel, and Jesse C. Vermaire. 2016. “The Effects of Migration on ca. 100-Year-Old Arsenic-Rich Mine Tailings in Cobalt, Ontario,

Canada." Environmental Earth Sciences 75 (5): 1–12. https://doi.org/10.1007/s12665-015-4898-1.

Sprague, Dale D., and Jesse C. Vermaire. 2018. "Legacy Arsenic Pollution of Lakes Near Cobalt, Ontario, Canada: Arsenic in Lake Water and Sediment Remains Elevated Nearly a Century After Mining Activity Has Ceased." Water, Air, and Soil Pollution 229 (87). https://doi.org/10.1007/s11270-018-3741-1.

Story Environmental. 2014. "Monitoring Well Logs - Nipissing Low Grade, Crosswise Lake, Cart Lake, Mile 104 Tailings."

Tyrell, J.B., Graham, R.P.D. 1913. "Yukonite, a new hydrous arsenate of iron and calcium from Tagish Lake, Yukon Territory, Canada; with a note on the associated symplesite." Transactions of the Royal Society of Canada: 7(4): 13-18.

Thayalakumaran, Thabo, Keith L. Bristow, Philip B. Charlesworth, and Thorsten Fass. 2008. "Geochemical Conditions in Groundwater Systems: Implications for the Attenuation of Agricultural Nitrate." Agricultural Water Management 95 (2): 103–15. https://doi.org/10.1016/j.agwat.2007.09.003.

Walker, Forest P., Madeline E. Schreiber, and J. Donald Rimstidt. 2006. "Kinetics of Arsenopyrite Oxidative Dissolution by Oxygen." Geochimica et Cosmochimica Acta 70 (7): 1668–76. https://doi.org/10.1016/j.gca.2005.12.010.

World Health Organization. 2011. "Arsenic in Drinking-Water. Background Document for Preparation of WHO Guidelines for Drinking-Water Quality." World Health Organization. https://apps.who.int/iris/bitstream/handle/10665/75375/WHO_SDE_WSH_03.04_75_eng.pdf?sequence=1&isAllowed=y.

Appendices

Appendix 1: Groundwater Elevation Contour Map (August 1991) (Dumaresq, 2005)

Appendix 2: Aqueous Geochemical Data

Appendix 3: EMPA Analytical Standards

Appendix 4: Photo Log

Appendix 1 - Groundwater Elevation Contour Map (August 1991) (Dumaresq, 2005)

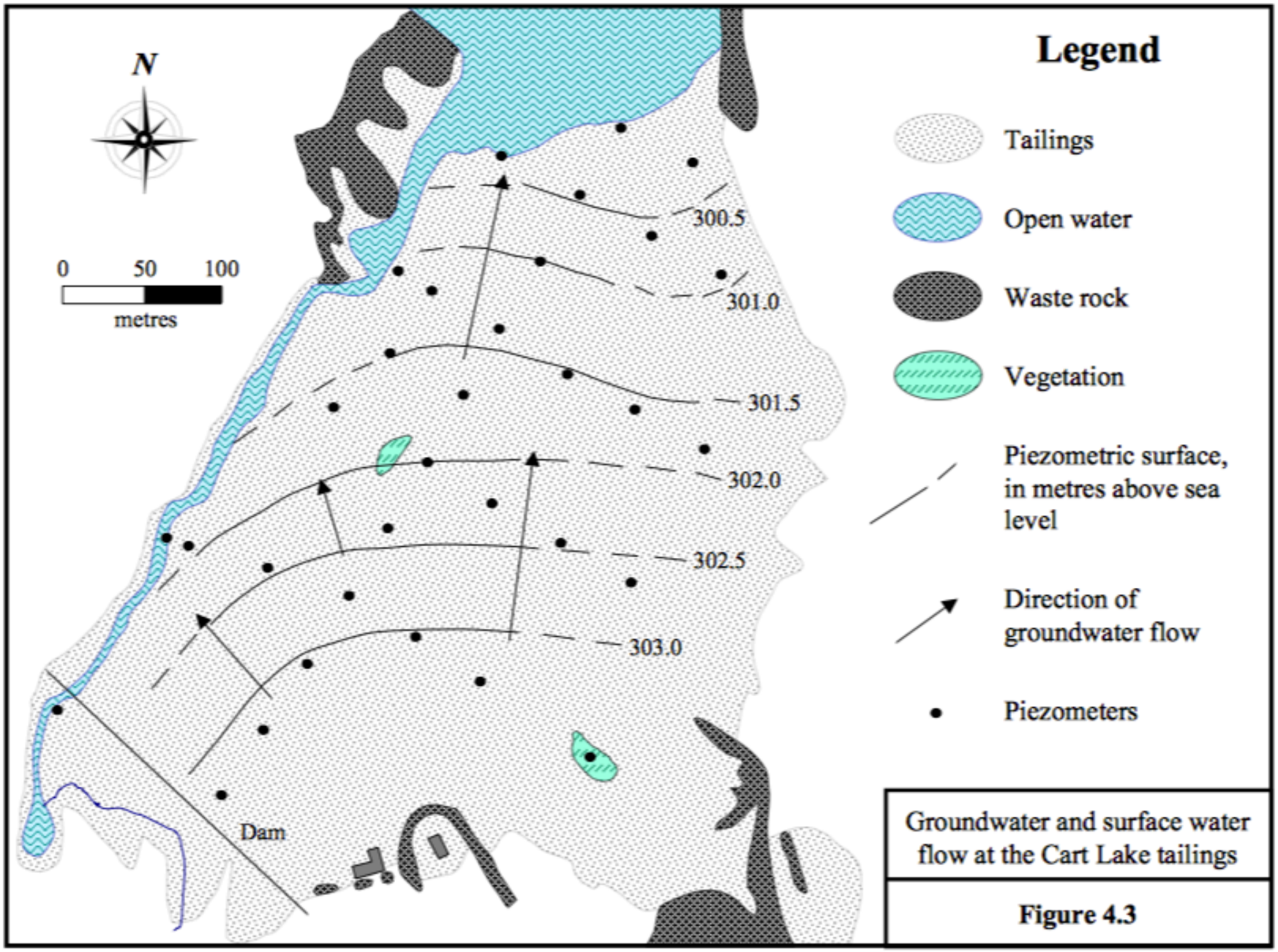

Appendix 2 – Aqueous Geochemical Data

Piezometer Samples – Cations

Sample ID	Ag	Al	As	Ba	Ca	Cd	Co	Cu	Fe	K	Mg	Mn	Mo	Na	Ni	Pb	Sb	Sr	Zn
CL-6	BD	0.00180	2.25671	0.06873	63.41600	BD	0.00908	0.00037	0.35069	3.22618	3.96119	0.02867	0.00439	3.29568	0.00672	0.00033	0.00433	0.06700	0.06827
CL-8	BD	0.00058	15.50503	0.12558	51.38800	0.00006	0.00030	0.00016	0.18900	3.51518	6.70399	0.10542	0.04841	7.57047	0.00127	BD	0.00064	0.11521	0.03012
CL-17S	BD	0.00118	0.00327	0.08927	75.30500	BD	BD	0.00017	2.56790	3.19612	4.35697	0.18318	BD	3.61099	0.00015	BD	BD	0.08320	0.00010
CL-17D	BD	0.00211	8.91731	0.12466	4.85280	0.00005	0.00467	0.00057	0.30654	1.13254	2.34301	0.00875	0.04478	8.75039	0.00422	0.00054	0.00489	0.02294	0.11276
CL-18	0.00021	0.01830	0.13769	0.09354	50.82000	0.00012	0.00652	0.00323	0.27018	2.35042	3.30636	0.07791	0.00159	6.49637	0.00396	0.00269	0.00092	0.06106	0.05362
CL-27	BD	0.00014	BD	0.17278	10.74800	BD	BD	0.00006	0.63528	2.96616	1.25801	0.06422	BD	2.09671	BD	BD	BD	0.01449	BD
MAX	0.00021	0.01830	15.50503	0.17278	75.30500	0.00012	0.00908	0.00323	2.56790	3.51518	6.70399	0.18318	0.04841	8.75039	0.00672	0.00269	0.00489	0.11521	0.11276
MIN	0.00021	0.00014	0.00327	0.06873	4.85280	0.00005	0.00030	0.00006	0.18900	1.13254	1.25801	0.00875	0.00159	2.09671	0.00015	0.00033	0.00064	0.01449	0.00010
MEDIAN	0.00021	0.00402	5.36400	0.11243	42.75497	0.00008	0.00514	0.00076	0.71993	2.73110	3.65492	0.07802	0.02479	5.30344	0.00326	0.00119	0.00270	0.06065	0.05297

Piezometer Samples – Anions and Field Parameters

Sample ID	Cl	F	NO3	PO4	SO4	Alkalinity (mg/L HCO_3^-)	Eh (mV)	pH
CL-6	0.35591	0.07909	0.26693	0.05438	72.93199	182.94176	209.19000	7.96000
CL-8	0.99431	0.21378	0.45241	0.06960	13.26413	201.99820	128.00000	7.75000
CL-17S	0.39990	0.11426	0.19216	0.05713	83.56404	148.64018	46.00000	7.78000
CL-17D	4.08290	0.24309	0.64493	0.04465	6.99500	45.73544	100.00000	7.22000
CL-18	0.62962	0.21487	2.53348	0.30981	58.73980	117.19707	207.23000	7.60000
CL-27	3.57314	0.16173	0.24259	9.63787	6.81272	91.47088	157.00000	6.75000
MAX	4.08290	0.24309	2.53348	9.63787	83.56404	201.99820	209.19000	7.96000
MIN	0.35591	0.07909	0.19216	0.04465	6.81272	45.73544	46.00000	6.75000
MEDIAN	1.67263	0.17114	0.72208	1.69557	40.38461	131.33059	141.23667	7.51000

Vertical Pore Water Profile Samples - Cations

Sample ID	Ag	Al	As	Ba	Ca	Cd	Co	Cu	Fe	K	Mg	Mn	Mo	Na	Ni	Pb	Sb	Sr	Zn
CL-TP01-0.1	BD	0.07939	1.14855	0.11048	90.94100	0.00005	0.01910	0.05447	0.11188	5.34933	3.98623	0.00363	0.01366	4.62891	0.01306	0.00255	0.04742	0.05082	0.04888
CL-TP01-0.2	0.00146	0.07002	0.95216	0.09995	94.23384	0.00011	0.03120	0.06803	0.09540	6.27858	4.36154	0.00392	0.02870	6.73267	0.01472	0.00294	0.05666	0.06576	0.04677
CL-TP01-0.3	BD	0.07408	5.44558	0.16741	34.58272	0.00012	0.01358	0.04806	0.08919	4.48925	1.61426	0.00288	0.02492	6.51835	0.00818	0.00252	0.12259	0.03070	0.03278
CL-TP01-0.4	BD	0.02971	3.48478	0.16995	45.25684	0.00008	0.01315	0.04930	0.01531	5.31366	2.41745	0.00473	0.03191	10.00740	0.01054	0.00079	0.14734	0.04111	0.03989
CL-TP01-0.5	0.00050	0.02667	4.47171	0.40820	35.75000	0.00002	0.00497	0.01880	0.00742	3.54507	2.25294	0.00189	0.00811	11.23130	0.00562	BD	0.18403	0.03731	0.00673
CL-TP01-0.6	0.00110	0.04033	7.71954	0.14722	34.05300	0.00004	0.01681	0.02725	0.03871	3.31441	1.55867	0.00303	0.01333	6.49989	0.01055	0.00213	0.26542	0.02681	0.02108
CL-TP01-0.7	BD	0.03831	7.88807	0.22742	34.56800	0.00003	0.01023	0.01018	0.02487	3.10761	1.93323	0.00357	0.00310	5.77596	0.00447	0.00066	0.18124	0.03013	0.01674
CL-TP01-0.8	BD	0.02763	13.89869	0.22392	39.28800	0.00001	0.01700	0.01698	0.00973	2.86206	2.04133	0.00367	0.00743	5.91697	0.00733	0.00031	0.26574	0.03414	0.01121
CL-TP01-0.9	0.00002	0.02304	11.63540	0.21560	41.37400	0.00002	0.01508	0.00379	0.00317	3.51330	1.65943	0.00166	0.00914	4.80361	0.00402	BD	0.29301	0.03462	0.01190
CL-TP01-1.0	BD	0.06011	18.09378	0.22644	35.62400	0.00002	0.01922	0.00633	0.05293	5.03866	1.33767	0.00173	0.00532	5.45815	0.00615	0.00089	0.36740	0.03161	0.01571
CL-BHW-0-20	0.00001	0.04964	8.95735	0.40261	39.82272	0.00004	0.00895	0.02173	0.04156	6.96284	2.50342	0.00554	0.00722	16.08937	0.00830	0.00129	0.21669	0.04687	0.02754
CL-BHW-20-40	0.00159	0.12076	5.86984	0.41918	22.42911	0.00003	0.00603	0.01126	0.07647	6.90755	1.23702	0.00286	0.00491	14.51601	0.00446	0.00408	0.29443	0.02971	0.02073
CL-BHW-40-60	0.00002	0.06087	15.98044	0.13647	30.16800	0.00003	0.01377	0.00826	0.02762	6.72523	2.19760	0.00156	0.01380	10.95810	0.00492	0.00104	0.43092	0.02969	0.01193
CL-BHW-60-80	BD	0.01894	7.00755	0.14843	79.48800	0.00010	0.14655	0.00493	BD	6.48152	4.46498	0.00723	0.05552	11.69670	0.03351	BD	0.50617	0.08439	0.04253
CL-BHW-80-100	BD	0.02856	9.22697	0.11880	192.0400	0.00015	0.24725	0.01047	0.00566	10.78610	8.67052	0.06602	0.05421	16.86410	0.06292	BD	0.61664	0.17659	0.11213
CL-BHW-100-120	BD	0.03470	10.96575	0.18503	43.43800	0.00010	0.02074	0.00297	0.01357	13.51810	3.50898	0.02266	0.09612	14.07650	0.06437	0.00030	2.07984	0.05278	0.02712
MAX	0.00159	0.12076	18.09378	0.41918	192.0400	0.00015	0.24725	0.06803	0.11188	13.51810	8.67052	0.06602	0.09612	16.86410	0.06437	0.00408	2.07984	0.17659	0.11213
MIN	0.00001	0.01894	0.95216	0.09995	22.42911	0.00001	0.00497	0.00297	0.00317	2.86206	1.23702	0.00156	0.00310	4.62891	0.00402	0.00030	0.04742	0.02681	0.00673
MEDIAN	BD	0.03932	7.80381	0.17749	39.55536	0.00004	0.01595	0.01412	BD	5.33149	2.22527	0.00360	0.01349	8.37003	0.00824	BD	0.26558	0.03596	0.02410

Vertical Pore Water Profile Samples – Anions and Field Parameters

Sample ID	Cl	F	NO3	PO4	SO4	Alkalinity (mg/L HCO_3^-)	Eh (mV)	pH
CL-TP01-0.1	3.50905	0.13498	120.0560	0.09487	31.39233	164.05814	412.00000	7.88000
CL-TP01-0.2	8.33094	0.15324	185.6655	0.19920	108.5252	32.23591	350.00000	8.14000
CL-TP01-0.3	7.22514	0.17405	6.20155	BD	44.53879	110.73674	387.00000	8.12000
CL-TP01-0.4	15.50755	0.00860	18.44698	BD	76.00442	44.42287	366.00000	8.55000
CL-TP01-0.5	9.03855	0.23951	1.33908	BD	19.25084	108.80103	368.00000	8.50000
CL-TP01-0.6	9.43071	0.14288	2.98806	BD	29.98620	139.30771	318.00000	8.27000
CL-TP01-0.7	2.32799	0.14145	9.37407	BD	6.95334	154.57093	344.00000	8.50000
CL-TP01-0.8	16.77924	0.23477	10.35280	BD	16.93883	120.92630	346.00000	8.29000
CL-TP01-0.9	1.24352	0.10878	2.55188	BD	20.60478	127.12329	399.00000	8.10000
CL-TP01-1.0	0.76571	BD	0.69235	BD	9.02098	133.23066	336.00000	8.60000
CL-BHW-0-20	5.24575	0.28146	1.79703	BD	21.20069	163.89833	364.00000	8.36000
CL-BHW-20-40	4.83757	0.13519	0.86730	BD	18.45234	170.01551	364.00000	8.36000
CL-BHW-40-60	3.55193	0.06467	2.41078	BD	26.55492	105.78514	345.00000	8.60000
CL-BHW-60-80	2.64167	0.07256	1.44358	0.22965	217.4086	90.49219	369.00000	8.13000
CL-BHW-80-100	1.62112	0.02360	1.61869	0.25847	456.1245	93.55078	350.00000	8.17000
CL-BHW-100-120	1.36300	BD	8.48948	0.40087	95.38974	96.60937	390.00000	8.04000
MAX	16.77924	0.28146	185.6655	0.40087	456.1245	170.01551	412.00000	8.60000
MIN	0.76571	0.00860	0.69235	0.09487	6.95334	32.23591	318.00000	7.88000
MEDIAN	4.19475	BD	2.76997	BD	28.27056	115.83152	363.22222	8.28278

Appendix 3 - EMPA Analytical Standards

Element/Line	Crystal	OnPeak Time	OffPeak Time	Standard	Analytical Error(rel%)	Detection Limit(99%)	Spectrometer	On-Peak Position	Hi-Off Position	Lo-Off Position	Gain	Bias
S ka	PETJ	20	20	Celestine	178.574	0.017157	1	171.679	176.178	167.181	16	1700
Fe ka	LIF	20	20	Hematite	2.85519	0.043376	3	134.702	138.648	130.756	32	1700
Cu ka	LIF	20	20	Cuprite	-72.636	0.065879	3	107.236	111.659	102.813	32	1700
Ni ka	LIFL	20	20	Pentlandite	5.39688	0.039354	4	115.362	119.447	111.278	32	1700
Co ka	LIFL	20	20	Cochromite	1.74377	0.037922	4	124.468	128.4	120.536	32	1700
As la	TAP	20	20	GaAs	1.10923	0.039445	5	105.103	113.339	96.8663	16	1700
Ca ka	PETJ	20	20	Diopside #1	2.22266	0.016927	1	107.168	112.857	101.478	16	1700
Al ka	TAP	20	20	Sanidine	1.70048	0.011549	2	90.464	99.382	81.5459	16	1700
Si ka	TAP	20	20	Sanidine	18.6648	0.010361	2	77.208	86.8558	67.5603	16	1700
Mn ka	LIFL	20	20	Tephroite	5.20684	0.029569	4	146.229	149.857	142.601	32	1700
K ka	PETJ	20	20	Sanidine	9.46224	0.017136	3	119.874	125.295	114.454	64	1700
Mg ka	TAP	20	20	Diopside #1	3.3818	0.01207	5	107.475	115.619	99.3299	16	1700

Appendix 4 – Photo Log

Photo 1: Aerial photo of Cart Lake

Photo 2: Silverfields mill at Cart Lake

Photo 3: Piezometer sampling

Photo 4: Piezometer sampling

Photo 5: Field parameter analysis at Cart Lake

Photo 6: Test pit for horizontal cores

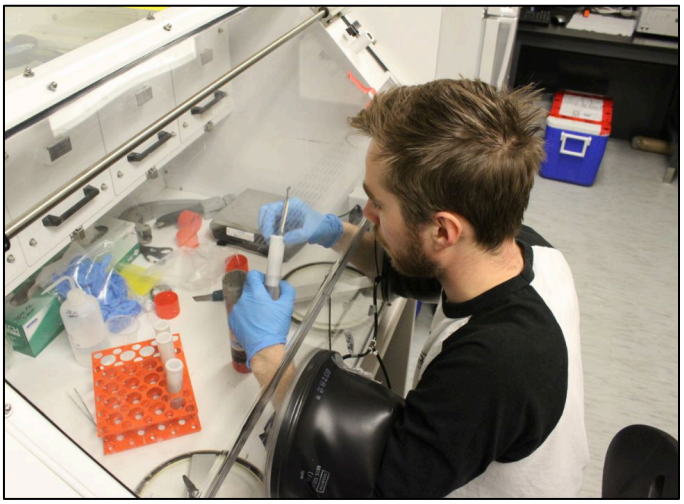

Photo 7: Anaerobic extraction for pore water analysis

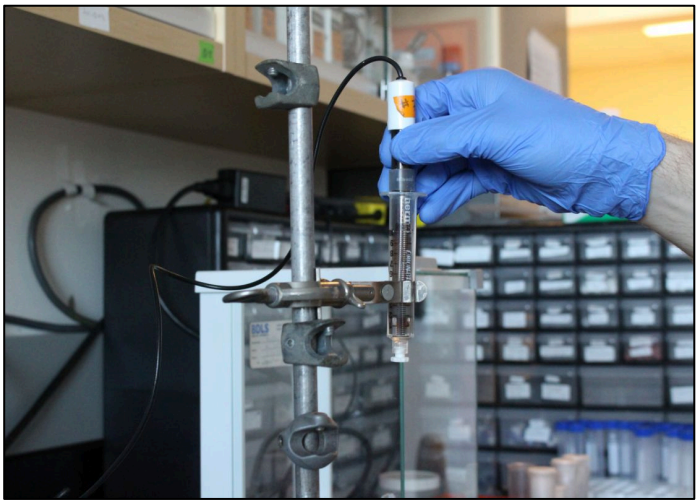

Photo 8: Field parameter analysis of extracted pore water

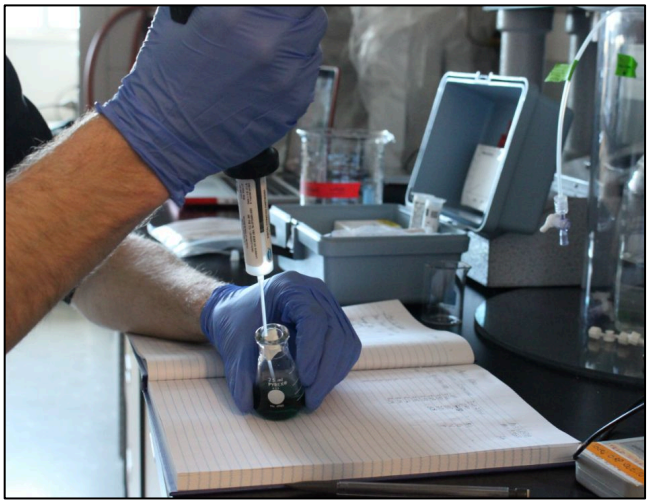

Photo 9: Lab titrations

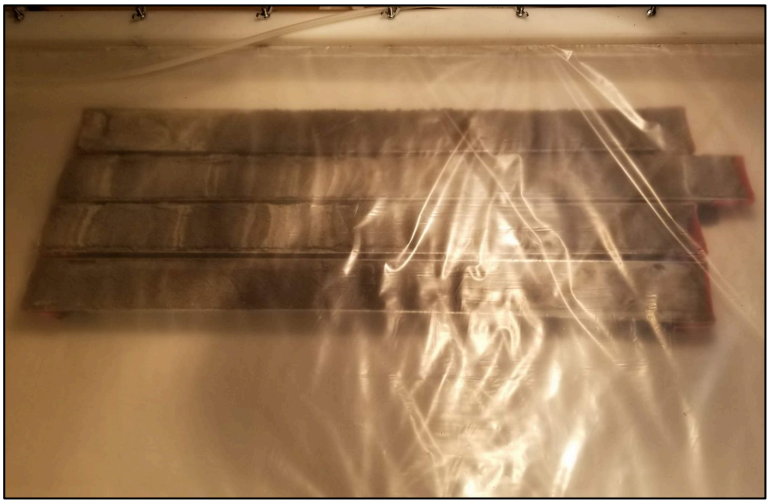

Photo 10: Core drying setup (cores)

Photo 11: Core drying setup (dessicant)

Photo 12: Thin sections prepared for cutting and polishing